NOAA Technical Memorandum ERL ETL-274

THE PROBABILITY DISTRIBUTION OF IRRADIANCE SCINTILLATION

Reginald J. Hill
Environmental Technology Laboratory

Rod G. Frehlich
Cooperative Institute for Research in Environmental Sciences (CIRES)
The University of Colorado/NOAA

William D. Otto
Environmental Technology Laboratory

Environmental Technology Laboratory
Boulder, Colorado
January 1997

UNITED STATES DEPARTMENT OF COMMERCE

Michael Kantor
Secretary

NATIONAL OCEANIC AND ATMOSPHERIC ADMINISTRATION

D. JAMES BAKER
Under Secretary for Oceans and Atmosphere/Administrator

Environmental Research Laboratories

James L. Rasmussen
Director

NOTICE

Mention of a commercial company or product does not constitute an endorsement by NOAA/ERL. Use for publicity or advertising purposes of information from this publication or concerning proprietary products or the tests of such products is not authorized.

CONTENTS

The Probability Distribution of Irradiance Scintillation

Reginald J. Hill, Rod G. Frehlich,[1] and William D. Otto

ABSTRACT. We calculated the probability distribution function (PDF) from simulations. The simulations were of an initially spherical wave propagated through homogeneous atmospheric turbulence. The onset of strong scintillation was calculated. By onset of strong scintillation, we mean conditions of weak scintillation changing to the condition of strong focusing. The simulations' PDFs are compared with several heuristic models of the PDF, and are seen to progress from close to lognormal for the cases of weakest scintillation to close to the lognormally modulated exponential PDF for the cases of strong scintillation. The simulations' PDFs are not in agreement with the K PDF for any of the calculated cases. The best agreement was obtained in comparison with Beckmann's PDF. Beckmann's PDF varies from being the lognormal PDF for weak scintillation to the lognormally modulated exponential PDF for strong scintillation, and progresses further to the theoretically expected exponential PDF in the limit of saturated scintillation.

1. INTRODUCTION

We used numerical simulation of the propagation of an initially spherical wave through homogeneous atmospheric turbulence to calibrate a new model of inner-scale and fluxes scintillometer (Hill et al., 1994). For this calibration, we calculated several irradiance statistics for conditions of weak to strong scintillation. A spin-off of such calculations is the probability distribution function (PDF) of irradiance scintillations. Here, we present the PDFs of irradiance and compare them with several current heuristic PDF models. Of particular interest is Beckmann's PDF, which we describe in detail in the next section. We also compare the irradiance PDF from the simulation with the well-known lognormal PDF, the lognormally modulated exponential PDF (Churnside and Hill, 1987), and the K PDF (Jakeman and Pusey, 1978). (The K PDF takes its name from the usual symbol, K, used for the modified Bessel function that appears in the formula for this PDF.)

2. BECKMANN'S PROBABILITY DISTRIBUTION FUNCTION

Beckmann (1967) derived a PDF for the amplitude of a wave propagating in a random medium. He found that the PDF is a Rice-Nakagami PDF (Nakagami, 1960) with a lognormal modulation. In honor of Petr Beckmann, we call this PDF "Beckmann's probability distribution," as did Milyutin and Yaremenko (1980). A more descriptive name, the "lognormally modulated Rician PDF," was used by Churnside and Clifford (1987) and Churnside and Frehlich (1989).

---

[1]Cooperative Institute for Research in Environmental Sciences (CIRES), University of Colorado/NOAA, Boulder, Colorado 80309.

The Rice-Nakagami PDF is

$$P_{RN}(I) = (r+1)\, z^{-1} \exp\left[-r-(r+1)\,\frac{I}{z}\right] I_0\left(\left\{4r\,[r+1]\,\frac{I}{z}\right\}^{1/2}\right), \qquad (1)$$

where I is the irradiance, z is the mean irradiance, and I_0 is the modified Bessel function (Abramowitz and Stegun, 1964). The lognormal PDF is

$$P_{LN}(z) = \frac{1}{\sqrt{2\pi}\,\sigma_z\, z} \exp\left[-\left(\ln z + \frac{1}{2}\,\sigma_z^2\right)^2 / 2\sigma_z^2\right], \qquad (2)$$

where σ_z^2 is the variance of $\ln z$, and the mean of z is unity. Beckmann's PDF is given by

$$P_B(I\,|\,r,\sigma_z^2) = \int_0^\infty dz\; P_{RN}(I\,|\,z,r)\; P_{LN}(z\,|\,\sigma_z^2)\;. \qquad (3)$$

Subscripts RN, LN, and B are used to refer to the Rice-Nakagami, lognormal, and Beckmann's PDFs, respectively. In (3), we list the parameters of the distribution on the right of the vertical bar and list the random variable on the left of the vertical bar.

In Sec. 5, we will show that Beckmann's PDF reduces to the lognormal PDF in the limit of weak scintillation. For very weak scintillation measured in the atmosphere, the lognormal PDF has been shown to be accurate (Gracheva et al., 1974; Hill et al., 1988). Churnside and Frehlich (1989) compared Beckmann's PDF with data from atmospheric scintillation obtained in very weak scintillation using a 50-m propagation path. They showed that it gives good agreement with the data for the locally stationary case, in fact, superior agreement compared with the IK PDF. The IK PDF was introduced by Andrews and Phillips (1985) as a generalization of the well-known K PDF (Jakeman and Pusey, 1978).

For strong scintillation, Churnside and Clifford (1987) showed that Beckmann's PDF reduces to the lognormally modulated exponential PDF (abbreviated LNME PDF). The LNME PDF was introduced by Churnside and Hill (1987), who gave a clear heuristic argument for applicability of the LNME PDF for the case of strong scintillation and showed that the LNME PDF is in good agreement with atmospheric scintillation data for the case of strong scintillation of a diverged wave on a 1000-m path. The LNME PDF is also in good agreement with numerical simulation of a diverged wave for the case of strong scintillation (Flatté et al., 1994). Although the LNME PDF is in better agreement with experiment and simulation for the case of strong scintillation of a diverged wave than is the K PDF (Churnside and Hill, 1987; Flatté et al., 1994), the LNME PDF is in somewhat worse agreement with simulation for the case of a plane wave than is the K PDF (Flatté et al., 1994). However, this does not necessarily imply that Beckmann's PDF is in worse agreement with plane-wave simulation than is the K PDF or the IK PDF; such comparisons have not yet been performed.

In the limit of saturated scintillation, it is well known that the PDF of irradiance becomes the exponential PDF (Little, 1951). Churnside and Hill (1987) showed that the LNME PDF reduces to the exponential PDF in the limit of saturated scintillations, as it should; therefore, Beckmann's PDF does also. Beckmann (1967), as well as Milyutin and Yaremenko (1980), has also shown that Beckmann's PDF reduces to the exponential PDF in the limit of saturated scintillations. For a diverged spherical wave and typical inner scale, the limit of saturated scintillation requires very long path lengths.

Since PDF models such as (3) have been found to be useful for engineering purposes as well as in studies of fundamental aspects of scintillation, and since Beckmann's PDF seems to be a particularly promising PDF for a very wide range of scintillation strengths from very weak to very strong, it is useful to determine the parameters of Beckmann's PDF. These parameters are r and σ_z^2. The former parameter r was named the coherence parameter by Churnside and Clifford (1987); the limits of very weak and very strong scintillation correspond to r approaching infinity and zero, respectively. Once the parameters have been determined in terms of the independent atmospheric parameters C_n^2, the refractive-index structure parameter, and ℓ_0, the inner scale of turbulence, then Beckmann's PDF can be used in modeling. Fante (1975) recommended Beckmann's PDF for such applications.

Milyutin and Yaremenko (1980) were the first to attempt to obtain the parameters of Beckmann's PDF in terms of C_n^2. However, they did not consider the effect of the inner scale, which has been shown to be important for quantitative prediction of scintillation for both weak (Hill and Ochs, 1978; Ochs and Hill, 1985; Azoulay et al., 1988; Frehlich, 1992; Hill, 1992; Thiermann and Grassl, 1992) and strong (Consortini et al., 1993; Flatté et al., 1993) atmospheric scintillation. The parameters determined by Milyutin and Yaremenko (1980) were neither as accurate as desired (even if $\ell_0 = 0$), nor did they present their results in terms of a minimum number of dimensionless parameters. Churnside and Clifford (1987) obtained the parameters of Beckmann's PDF in terms of the predictions of the heuristic theory of logamplitude variance. The heuristic theory was originated by Clifford et al. (1974) and was later refined by Hill and Clifford (1981) and Hill (1982) to include the effects of inner scale. However, we have shown that this heuristic theory is not as accurate as is desirable (Hill and Frehlich, 1996). It is shown in the Appendix that the values of r and σ_z^2 given by Churnside and Clifford (1987) are not accurate.

3. STATISTICS FROM BECKMANN'S PDF

To obtain r and σ_z^2 from irradiance statistics, we must establish the following relationships. Recall that for any PDF, $P(I)$ the moments of irradiance are given by

$$\langle I^n \rangle = \int_0^\infty dI\; I^n\, P(I)\;. \qquad (4)$$

Angle brackets denote the average of the quantity within. The irradiance moments of the RN PDF are easily obtained from (1), (4), and tabulated integrals:

$$<I^n>_{RN} = \frac{z^n}{(r+1)^n} \sum_{m=0}^{n} (n!/m!)^2 \frac{r^m}{(n-m)!} , \tag{5}$$

from which we obtain the first and second moments:

$$<I>_{RN} = z \tag{6a}$$

$$<I^2>_{RN} = z^2 (r^2 + 4r + 2)/(r+1)^2 . \tag{6b}$$

Applying (4) to Beckmann's PDF (3), we immediately obtain (5) within the integration over z, and this integration is immediately identified as the moments of the lognormal PDF. Thus, we obtain the moments of Beckmann's PDF:

$$<I^n>_B = (r+1)^{-n} \exp\left[\frac{1}{2} n(n-1)\sigma_z^2\right] \sum_{m=0}^{n} (n!/m!)^2 \frac{r^m}{(n-m)!} , \tag{7}$$

which verifies Eq. (8) by Churnside and Clifford (1987), despite their misprint in their definition of Beckmann's PDF. The mean of the logarithm of irradiance for any PDF is given by

$$\langle \ln I \rangle = \int_0^\infty dI \ln I \, P(I) . \tag{8}$$

The logarithm of irradiance is hereafter referred to as log-irradiance. Applying (8) to the RN PDF (1) and using Eq. (5) in Sec. 2.15.12 of Prudnikov et al. (1986), we obtain

$$\langle \ln I \rangle_{RN} = g(r) + \ln z , \tag{9}$$

where

$$g(r) \equiv \ln[r/(r+1)] + E_1(r) \tag{10}$$

and the exponential integral function is defined by

$$E_1(r) \equiv \int_r^\infty dt \, t^{-1} e^{-t} \tag{11}$$

(cf., Abramowitz and Stegun, 1964). Applying (8) to Beckmann's PDF, we obtain (9) within the integration over z and perform the integration by recognizing the normalization and mean log-irradiance of the lognormal PDF. We determine that the mean of the log-irradiance from Beckmann's PDF is

$$\langle \ln I \rangle_B = g(r) - \frac{1}{2}\sigma_z^2 . \tag{12}$$

Integral tables do not allow us to express the variance of log-irradiance as an analytic formula analogous to (12). From the irradiance moments (7), we obtain

$$<I>_B = 1 , \tag{13}$$

which expresses the normalization of the irradiance, and

$$<I^2>_B = e^{\sigma_z^2}(r^2 + 4r + 2)/(r+1)^2 . \tag{14}$$

The moment $<I^{\mu-1/2}>$ for $\mu - 1/2 > -1$, where μ is a real number, can also be calculated for Beckmann's PDF by use of formulas in Sec. 6.64 of Gradshteyn and Ryzhik (1965). As the first step for the RN PDF, we obtain

$$<I^{\mu-1/2}>_{RN} = G_\mu(r) \, z^{\mu-1/2} , \tag{15}$$

where

$$G_\mu(r) \equiv r^{-1/2}(r+1)^{-\mu+1/2} e^{-r/2} \Gamma(\mu+1/2) M_{-\mu,0}(r) , \tag{16}$$

Γ is the gamma function, and $M_{-\mu,0}$ is a Whittaker function given in Secs. 9.22 and 9.23 of Gradshteyn and Ryzhik (1965). Applying (4) with n replaced by $\mu - 1/2$ to Beckmann's PDF, we obtain $z^{\mu-1/2}$ within the integration over z, which is performed by noting that for p, a real number,

$$\langle z^p \rangle_{LN} = \exp\left[\frac{1}{2} p(p-1)\sigma_z^2\right] . \tag{17}$$

Therefore, for Beckmann's PDF we have the statistic

$$<I^{\mu-1/2}>_B = G_\mu(r) \exp\left[\frac{1}{2}\left(\mu - \frac{1}{2}\right)\left(\mu - \frac{3}{2}\right)\sigma_z^2\right] , \tag{18}$$

provided that $\mu - 1/2 > -1$. In particular, for $\mu = 0$, we use the relationship of $M_{0,0}$ to the modified Bessel function to determine that

$$<I^{-1/2}>_B = G_0(r) \exp(3\sigma_z^2/8) , \tag{19}$$

where

$$G_0(r) = \pi^{1/2}\,(r+1)^{1/2}\,e^{-r/2}\,I_0(r/2)\ . \tag{20}$$

4. DETERMINING THE PARAMETERS r AND σ_z^2 OF BECKMANN'S PDF

We define the following parameters: λ is the wavelength of the radiation; L is the length of the propagation path; $R_F = \sqrt{L/k}$ is the Fresnel distance; C_n^2 is the refractive-index structure parameter; and ℓ_0 is the inner scale of turbulence. The inner scale is the spacing at which the asymptotic formula for the inertial-convective range of the refractive-index structure function equals its asymptotic dissipation-range formula (cf., Hill and Clifford, 1978). The refractive-index spectrum is denoted by $\Phi_n(\kappa)$, where κ is the spatial wave number. A dimensionless function $H(\kappa\,\ell_0)$ describes the spectral bump and dissipation range of $\Phi_n(\kappa)$. In effect, $H(\kappa\,\ell_0)$ is defined through the relationship

$$\Phi_n(\kappa) = 0.033\,C_n^2\,\kappa^{-11/3}\,H(\kappa\,\ell_0)\ .$$

We call the irradiance variance in the weak-scintillation limit the Rytov variance and denote it by σ^2_{Rytov}. In this limit of very weak scintillation, we have

$$\sigma^2_{\text{Rytov}} = \sigma_I^2 = \sigma^2_{\ln I} = -2\left\langle \ln I \right\rangle\ .$$

Formulas for σ^2_{Rytov} in terms of $\Phi_n(\kappa)$ for a spherical wave propagating through isotropic turbulence that is homogeneous along the propagation path are given, for instance, by Eqs. (T8) and (T26) of Lawrence and Strohbehn (1970). Let $x = \kappa R_F$ be the dimensionless wave number, and let u be the propagation-path position normalized by path length; thus, u varies from 0 at the transmitter to 1 at the receiver. Then, (T26) of Lawrence and Strohbehn can be expressed as (cf., Hill and Frehlich, 1996)

$$\sigma^2_{\text{Rytov}} = \beta_0^2\,\tilde{\sigma}^2(\ell_0/R_F)\ , \tag{21a}$$

where

$$\beta_0^2 \equiv 0.496\,k^{7/6}\,L^{11/6}\,C_n^2 \tag{21b}$$

and

$$\tilde{\sigma}^2(\ell_0/R_F) \equiv 10.5\int_0^1 du \int_0^\infty dx\,x^{-8/3}\,H(x\,\ell_0/R_F)\,\sin^2\left[x^2\,u\,(1-u)/2\right]\ . \tag{21c}$$

The quantity β_0^2 is the weak-scintillation variance for an inertial range extending over all wave numbers (i.e., for $\ell_0 = 0$). Thus, $\tilde{\sigma}^2(0) = 1$. The dimensionless function $\tilde{\sigma}^2(\ell_0/R_F)$ is manifestly a function of only its one dimensionless argument. Thus, $\tilde{\sigma}^2(\ell_0/R_F)$ gives the effect on scintillation of the spectral bump and dissipation range of $\Phi_n(\kappa)$; in other words, it gives the inner-scale effect.

The dimensionless quantities σ^2_{Rytov} and ℓ_0/R_F are used to present our PDFs. Hill and Frehlich (1996) showed that only two dimensionless parameters are needed to determine the irradiance and log-irradiance statistics even for arbitrary strength of scintillation.

The logarithm of (14) is

$$\ln \langle I^2\rangle_B = \sigma_z^2 + \ln\left[(r^2+4r+2)\big/(r+1)^2\right]\ . \tag{22}$$

From (10), (12), and (22), we have

$$2\,E_1(r) + \ln\left[r^2\,(r^2+4r+2)\big/(r+1)^4\right] = 2\left\langle \ln I\right\rangle + \ln(\langle I^2\rangle)\ , \tag{23}$$

which is easily solved numerically for r. On the right side of (23), we substitute the statistics from our simulation, namely, $\langle \ln I\rangle$ and $\langle I^2\rangle$. That is, we are requiring that $\langle \ln I\rangle_B = \langle \ln I\rangle$ and $\langle I^2\rangle_B = \langle I^2\rangle$. Knowing r, we can obtain σ_z^2 from either (12) or (22); that is, either

$$\sigma_z^2 = 2\,g(r) - 2\left\langle \ln I\right\rangle \tag{24a}$$

or

$$\sigma_z^2 = \ln\left[\langle I^2\rangle\,(r+1)^2\big/(r^2+4r+2)\right]\ . \tag{24b}$$

Alternatively, we can use the moments $\langle I^2\rangle$ and $\langle I^{-1/2}\rangle$ to determine r and σ_z^2. If we combine (19) with (14), we obtain

$$\left[G_0(r)\right]^{-8/3}\,(r^2+4r+2)/(r+1)^2 = \langle I^{-1/2}\rangle^{-8/3}\,\langle I^2\rangle\ . \tag{25}$$

This can be easily solved for r given that the right-hand side of (25) is assigned the value obtained from the simulation. Then, σ_z^2 can be obtained from either (14) or (19).

In Table 1, we give r and σ_z^2 for the values of ℓ_0/R_F and Rytov variance σ^2_{Rytov}, for which Hill and Frehlich (1996) performed simulations. A wide range of ℓ_0/R_F is given, but Rytov variance is given for values less than the maximum of σ_I^2. That is, Table 1 gives r and σ_z^2 for the weak scintillation side of the strong focusing region, although σ_I^2 reached values as large as 10 in the simulations performed by Hill and Frehlich (1996). As discussed by Hill and Frehlich

TABLE 1. Values of r (top number) and σ_z^2 (bottom number) for various values of ℓ_0/R_F and σ^2_{Rytov}. All values were obtained from the simulation's values of $<\ln I>$ and $<I^2>$, with the exception of the upper right corner, for which $<I^{-1/2}>$ and $<I^2>$ were used. An asterisk means that no pair of moments gave a solution for r in the range 0 to ∞. The second column contains values calculated from (21c).

ℓ_0/R_F	$\tilde{\sigma}^2$	σ^2_{Rytov}								
		0.06	0.12	0.20	0.40	0.70	1.00	1.30	2.00	3.00	5.00
0.00	1.00	53.90580	26.61605	15.67765	7.45918	3.87702	2.40635	1.59939	0.62938	*	0.32906
		0.02305	0.04585	0.07568	0.14697	0.24195	0.32173	0.38819	0.50353	*	0.80482
0.12	1.11	49.96704	24.70610	14.54831	6.91681	3.58041	2.20493	1.45042	0.53451	*	0.18168
		0.02116	0.04212	0.06953	0.13492	0.22100	0.29216	0.35128	0.45378	*	0.71655
0.16	1.16	50.43898	24.88977	14.66282	6.96973	3.60689	2.21532	1.44693	0.47269	*	*
		0.02132	0.04252	0.07017	0.13613	0.22296	0.29437	0.35294	0.44822	*	*
0.20	1.21	51.21155	25.29707	14.89172	7.07911	3.66301	2.24639	1.45832	0.41213	*	*
		0.02179	0.04340	0.07166	0.13893	0.22766	0.30035	0.35926	0.44756	*	*
0.30	1.27	54.01931	26.71010	15.71816	7.46180	3.86287	2.36368	1.52023	0.26499	*	*
		0.02361	0.04696	0.07747	0.15012	0.24626	0.32486	0.38720	0.45951	*	*
0.40	1.27	57.80313	28.51663	16.77302	7.94401	4.11147	2.51810	1.61410	0.13002	*	*
		0.02596	0.05160	0.08501	0.16458	0.27035	0.35714	0.42501	0.48517	*	*
0.50	1.22	62.63270	30.86806	18.11905	8.55794	4.42626	2.71904	1.75226	0.24122	*	*
		0.02858	0.05675	0.09342	0.18049	0.29678	0.39291	0.46822	0.53997	*	*
0.60	1.16	68.95416	33.91330	19.85028	9.33218	4.81652	2.96944	1.93374	0.42510	*	*
		0.03145	0.06234	0.10253	0.19759	0.32490	0.43099	0.51500	0.60870	*	*
0.70	1.08	77.53686	37.95094	22.14813	10.32922	5.30168	3.27676	2.15703	0.61793	*	*
		0.03458	0.06846	0.11235	0.21599	0.35474	0.47125	0.56454	0.68107	*	*
0.80	0.99	90.13691	43.76593	25.37013	11.67967	5.92450	3.65866	2.43313	0.82786	*	*
		0.03808	0.07515	0.12311	0.23587	0.38626	0.51330	0.61628	0.75507	*	*
1.00	0.81	154.35740	70.89755	39.25326	16.72393	7.89708	4.74289	3.16935	1.29147	*	*
		0.04733	0.09240	0.15017	0.28395	0.45857	0.60625	0.72816	0.90476	*	*
1.30	0.62	*	*	*	*	33.38438	9.56606	5.47392	2.25400	*	*
		*	*	*	*	0.63434	0.78245	0.91901	1.12778	*	2.44316
2.50	0.20	*	*	*	*	*	*	*	*	*	1.85184
		*	*	*	*	*	*	*	*	*	*

(1996), only two dimensionless parameters determine all irradiance statistics for practically the entire range of atmospheric-turbulence cases of interest. We have chosen the two parameters to be ℓ_0/R_F and σ^2_{Rytov} because these dimensionless parameters efficiently display the irradiance statistics (Hill and Frehlich, 1996) and therefore also provide an orderly variation to r and σ_z^2 that is amenable to interpolation.

However, the Rytov variance depends on both C_n^2 and ℓ_0, as is evident from (21a–c). The second column in Table 1 gives values of $\tilde{\sigma}^2$. Given an experiment in which k, L, C_n^2, and ℓ_0 are specified, one can immediately determine ℓ_0/R_F and β_0^2. The second column in Table 1 then gives $\tilde{\sigma}^2$ from the value of ℓ_0/R_F. Then (21a) gives the Rytov variance. Next, Rytov variance and ℓ_0/R_F determine r and σ_z^2 from Table 1. Finally, Beckmann's PDF can be computed by numerical integration of (3).

All values in Table 1 were obtained from $<\ln I>$ and $<I^2>$, with the exception of the upper right corner of Table 1, for which $<I^{-1/2}>$ and $<I^2>$ were used. The asterisks in Table 1 indicate that no solution for r was found no matter what combination of two statistics was tried, including $<I^3>$ and $<I^2>$. For instance, for the rightmost two columns in Table 1, the asterisks correspond to the right-hand side of (23) being less than the lower permissible limit of the left-hand side, namely, -0.4613. This lower limit corresponds to $r = 0$, which corresponds to Beckmann's PDF becoming the LNME PDF. Thus, the LNME PDF should serve as a replacement for Beckmann's PDF in these cases. On the other hand, the asterisks in the bottom two rows of all but the two rightmost columns in Table 1 correspond to the right-hand side of (23) being greater than the upper permissible limit of the left-hand side, namely, zero. This upper limit corresponds to $r = \infty$, which corresponds to Beckmann's PDF becoming the lognormal PDF. Thus, the lognormal PDF should serve as a replacement for the Beckmann PDF in these cases. However, the lower right corner of Table 1 apparently contains cases for which neither limiting form of Beckmann's PDF is accurate, as will be demonstrated by subsequent figures.

5. ASYMPTOTIC FORMULAS FOR BECKMANN'S PDF

Whereas Milyutin and Yaremenko (1980) and Fante (1975) stated without proof that Beckmann's PDF becomes the lognormal PDF in the limit of very weak scintillation, they did not state whether or not their result requires the scintillation to be so weak that Beckmann's PDF and the lognormal PDFs must both be approaching the Gaussian PDF. Strohbehn et al. (1975) showed that the RN PDF becomes nearly the same as the lognormal PDF, but that the two PDFs are only asymptotically equal for the case of such weak scintillation that both PDFs approach the Gaussian PDF. The analysis by Churnside and Clifford (1987) suggested that Beckmann's PDF does not quite become the lognormal PDF for weak scintillation. Beckmann (1967) showed in his Sec. 4.5 that for weak scattering his PDF approaches the rightmost PDF within the integral in (3), which is denoted by P_{LN} in (3). He showed that this is true even if P_{LN} is an arbitrary PDF,

not just the lognormal PDF, provided that a certain order of integrations can be reversed. A different proof that Beckmann's PDF becomes the lognormal PDF for weak scintillation is given here.

The approach to the weak scintillation limit is obtained when the coherence parameter r tends to infinity. This is seen from the fact that the right-hand side of (23) vanishes if I becomes a lognormal random variable, and that solution of (23) is $r = \infty$ as the right-hand side of (23) tends to zero. In the summation within (7), only the $m = n$ term contributes as $r \to \infty$, in which case (7) becomes

$$\langle I^n \rangle_B \to \exp\left[\frac{1}{2}\, n\,(n-1)\,\sigma_z^2\right] = \langle I^n \rangle_{LN}\,, \tag{26}$$

which is recognized as the moments of the lognormal PDF. However, the lognormal PDF is not determined by its moments of all orders (Strohbehn et al., 1975). Thus, (26) cannot be taken as proof that Beckmann's PDF approaches the lognormal PDF.

As $r \to \infty$ in (1), $P(I)$ becomes vanishingly small unless I is restricted to values very near its mean z; hence, the argument of the modified Bessel function becomes very large. We use the asymptotic expansion of the modified Bessel function for a large argument, neglect unity relative to r, substitute (1) and (2) in (3), and change the integration variable to $x = \sqrt{I/z}$; we thereby obtain

$$P_B(I) \to \frac{r^{1/2}}{\pi\sqrt{2}\,\sigma_z\, I} \int_0^\infty dx \exp\left[-r\,(1-x)^2 + \frac{1}{2}\ln x - \frac{(\ln I + \frac{1}{2}\,\sigma_z^2 - 2\ln x)^2}{2\,\sigma_z^2}\right]. \tag{27}$$

As $r \to \infty$, the integral in (27) is increasingly dominated by values of x very close to unity; in fact, $(1-x)^2$ must be of the order of r^{-1} as $r \to \infty$. Thus, we may neglect $\ln(x)$ within the integrand. After a change of integration variable to $t = \sqrt{r}\,(x-1)$, we have

$$P_B(I) \to \frac{1}{\pi\sqrt{2}\,\sigma_z\, I} \exp\left[-\left(\ln I + \frac{1}{2}\,\sigma_z^2\right)^2 \Big/ 2\,\sigma_z^2\right] \int_{-\sqrt{r}}^{\infty} dt\, e^{-t^2}. \tag{28}$$

As $r \to \infty$, the remaining integral in (28) approaches $\sqrt{\pi}$, and we see that (28) becomes (2). In (28), the variance of $\ln I$ is given by σ_z^2, and $\langle \ln I \rangle = -\sigma_z^2/2$ because $\langle I \rangle = 1$. Therefore, Beckmann's PDF becomes the lognormal PDF for weak scintillation.

The essential property of (3) is that the one PDF, denoted by P_{RN}, has a single maximum such that it becomes the Dirac delta function $\delta(z-I)$ as its variance goes to zero, and that the second PDF, denoted by P_{LN}, is modulating the mean, but not the variance, of the first PDF.

Given this property, the integrand in (3) becomes $\delta(z-I)\,P_{LN}(z)$ as the variance of the first PDF goes to zero. Therefore, the integral over z in (3) is evaluated to give the first PDF.

6. PROBABILITY DISTRIBUTION FUNCTIONS CALCULATED FROM SIMULATIONS

Our simulations used the spherical-wave algorithm described by Coles et al. (1995). The Fresnel distance was 10 grid points. For each realization, we used 20 screens along the propagation path. For the cases $\sigma^2_{Rytov} \le 2.0$, we used 512×512 grid points per phase screen, and 50 realizations were averaged to produce each PDF. For cases in which $\sigma^2_{Rytov} = 5.0$, we used 1024× 1024 grid points per screen, and 15 realizations were averaged to produce each PDF. Thus, the number of partially correlated irradiance values producing the PDFs was 512×512× 50 = 13,107,200, and 1024×1024×15 = 15,728,640 for the former and latter cases, respectively.

We determine the parameter of the K PDF and of the LNME PDF from the simulations' values of $\langle I^2 \rangle$. Since $\langle I^2 \rangle$ is determined more by large values of $\ln I$ (i.e., by large values of I) than by small values of $\ln I$, it follows that the K and LNME PDFs will fit the simulations' PDFs better at larger $\ln I$ than at smaller $\ln I$. Had we chosen to fit these PDFs to the simulation by using statistics such as $\ln I$ and $\langle I^{-1/2} \rangle$, then these PDFs would fit the simulation better at small $\ln I$ because $\langle \ln I \rangle$ and $\langle I^{-1/2} \rangle$ are determined more by small values of $\ln I$ than by large $\ln I$. To determine the parameters of Beckmann's PDF, we used the simulations' values of $\langle \ln I \rangle$ and $\langle I^2 \rangle$, except for one case for which we used $\langle I^{-1/2} \rangle$ and $\langle I^2 \rangle$; this one case is in the far upper right-hand corner of Table 1. Thus, Beckmann's PDF is fit by one statistic that is determined by relatively smaller values of $\ln I$ and one that is determined by larger $\ln I$.

The variance of log-irradiance is defined by

$$\sigma^2_{\ln I} \equiv \left\langle \left(\ln I - \langle \ln I \rangle\right)^2 \right\rangle .$$

We define σ by the square root of the value of $\sigma^2_{\ln I}$ as determined from a simulation. That is,

$$\sigma \equiv \sqrt{\sigma^2_{\ln I}}\,, \tag{29}$$

provided that a simulation determined $\sigma^2_{\ln I}$. In contrast, the K, LNME, and Beckmann's PDFs have values of $\sigma^2_{\ln I}$ that differ from σ^2 because the parameters of these PDFs were not determined to constrain $\sigma^2_{\ln I}$ to equal that of a simulation. On the other hand, we determine the lognormal PDF such that its value of $\sigma^2_{\ln I}$ equals σ^2. We use σ to scale the ordinates and abscissas of our figures.

The PDF of $\ln I$ from the simulation data was binned using 2000 bins equally spaced in $\ln I$ from $\ln I = -15$ to 5. We call these bins the elemental bins. No events occurred beyond the bin limits of -15 and 5. For presentation of our figures, we reduce the number of bins to be graphed by averaging the PDF over adjacent elemental bins to produce a single final bin. For $\sigma^2_{\text{Rytov}} = 0.06$, five adjacent elemental bins were averaged to produce final bins, and all final bins are plotted. For $\sigma^2_{\text{Rytov}} \geq 1.0$, ten adjacent elemental bins were averaged to produce final bins, and every other final bin is plotted. Furthermore, below a threshold probability level we added yet more adjacent elemental bins in order to maintain a minimum number of events in each final bin. For $\sigma^2_{\text{Rytov}} = 0.06$, the threshold was 5×10^{-5}, and for the other cases it was 10^{-3}. Thus, the final bins may become larger than 5 or 10 (as the case may be) of the elemental bins at a probability level below the threshold. (For the journal version of the figures, we use the same procedure for $\sigma^2_{\text{Rytov}} = 0.06$, but for $\sigma^2_{\text{Rytov}} \geq 1.0$ we average 20 elemental bins to form final bins and plot all final bins; the thresholds are unchanged.)

If there were insufficient remaining events in all the remaining lowest probability elemental bins, then the binning into final bins ceased. For the small values of $\ln I$, the total probability beyond the final bin of lowest probability is a cumulative probability given by

$$P\left[\ln I < (\ln I)_i\right] = \sum_{j=0}^{i-1} P\left[(\ln I)_j\right], \tag{30a}$$

where j is the index of the elemental bins and i is the index of the last elemental bin included in the final bin having the smallest value of $\ln I$. Likewise, for the large values of $\ln I$, the total probability beyond the final bin of lowest probability is a cumulative probability given by

$$P\left[\ln I > (\ln I)_k\right] = \sum_{j=k+1}^{2000} P\left[(\ln I)_j\right], \tag{30b}$$

where j is again the index of the elemental bins and k is the index of the last elemental bin included in the final bin having the largest value of $\ln I$. In Tables 2 and 3, we give the values of the cumulative probabilities (30a,b) multiplied by σ and the values of XL and XH, which are the abscissa values defined by

$$XL \equiv [(\ln I)_i + 0.5\,\sigma^2]/\sigma, \tag{31a}$$

$$XH \equiv [(\ln I)_k + 0.5\,\sigma^2]/\sigma. \tag{31b}$$

Figure 1 shows the line symbol key for the subsequent figures. The subsequent figures have an inset showing the details of the curves near the peak of the PDFs, as well as an inset showing the corresponding values of σ^2_{Rytov}, ℓ_0/R_F, β_0^2, and σ. Each simulation's PDF is graphed as circles with the ordinate value equal to the probability of the final bins multiplied by σ and with abscissa values equal to $(\ln I + 0.5\,\sigma^2)/\sigma$, wherein $\ln I$ is the center of the final bins. The curves for the heuristic PDFs are, in fact, line segments that connect points having abscissa

TABLE 2. The simulations' cumulative probability (top numbers) that is beyond the leftmost elemental bins included in Figs. 2–10 and the abscissas' values of those leftmost elemental bins (bottom numbers). The top and bottom numbers are calculated from (30a) multiplied by σ and (31a), respectively.

	σ^2_{Rytov}			
ℓ_0/R_F	0.06	1.0	2.0	5.0
0.0	1.69 E-5	5.19 E-4	8.63 E-5	6.49 E-4
	-5.590	-9.654	-9.516	-7.557
0.5	3.01 E-5	4.72 E-4	7.33 E-4	540 E-4
	-4.968	-9.622	-8.020	-7.096
1.0	0	2.83 E-4	2.72 E-4	5.07 E-4
	-4.581	-9.314	-8.531	-6.535

TABLE 3. The simulations' cumulative probability (top numbers) that is beyond the rightmost elemental bins included in Figs. 2–10 and the abscissas' values of those rightmost elemental bins (bottom numbers). The top and bottom numbers are calculated from (30b) multiplied by σ and (31b), respectively.

	σ^2_{Rytov}			
ℓ_0/R_F	0.06	1.0	2.0	5.0
0.0	2.44 E-5	4.02 E-4	3.24 E-5	7.87 E-4
	4.291	3.406	3.475	3.458
0.5	3.39 E-5	3.97 E-4	5.77 E-4	1.08 E-4
	4.485	3.506	3.343	3.579
1.0	2.62 E-5	9.42 E-4	8.71 E-4	4.36 E-4
	5.030	3.755	3.604	3.443

line symbol	PDF's name
o o o o o o o o o o o o o o o o o o o o	Simulation
– — — — — — — — — —	Beckmann
-·—·-·—·-·—·-·—·-·—·-	LNME
--·—·--·—·--·—·--·—·--·—·--	K
———————————————	Lognormal

FIGURE 1. Key to line symbols in Figs. 2–5.

values equal to those of the centers of the final bins and having ordinate values equal to the heuristic model's probability integrated over the final bins and multiplied by σ. Thus, on each figure, the simulation's and heuristic PDFs are all graphed as histograms having identical bins. On some of the figures, one can see a PDF end within the plotting area; this is because the end point is at the center of the leftmost or rightmost final bin and no final bins exist beyond that bin.

Our figures are very similar in appearance to those by Flatté et al. (1994). However, our choice of ordinate and abscissa differs from that by Flatté et al. (1994) and therefore requires some explanation. Flatté et al. (1994) presented the PDFs versus $(\ln I - \langle \ln I \rangle)/\sigma_{\ln I}$, where $\langle \ln I \rangle$ and $\sigma_{\ln I} \equiv \sqrt{\sigma^2_{\ln I}}$ differ for each PDF plotted. For instance, the exponential PDF has unit mean irradiance, $\sigma_{\ln I} = \pi/\sqrt{6}$, and $\langle \ln I \rangle = -\gamma \approx -0.58$, where γ is Euler's number. The curves plotted by Flatté et al. (1994) are their PDFs multiplied by their PDFs' respective value of $\sigma^2_{\ln I}$. Plotting the exponential PDF multiplied by $\pi/\sqrt{6}$ and using $(\ln I + \gamma)/(\pi/\sqrt{6})$ as the abscissa results in the same curve on all graphs. The lognormal PDF has unit mean irradiance and $\langle \ln I \rangle = 0.5\,\sigma^2_{\ln I}$. For the lognormal PDF, Flatté et al. (1994) took $\sigma^2_{\ln I}$ to be their simulation's value for each graph; thus, the lognormal PDF is also the same curve on all their graphs. However, where the curves for the exponential and lognormal cross on the graphs by Flatté et al. (1994) does not imply that the two PDFs are equal. Let A be the abscissa value for which their curves for these two PDFs have a crossing. For the lognormal PDF, the value of $\ln I$ corresponding to the abscissa value A is obtained by solving $[(\ln I)_{LN} + 0.5\,\sigma^2_{\ln I}]/\sigma_{\ln I} = A$, whereas for the exponential PDF a different value of $\ln I$ corresponding to the same abscissa value is obtained by solving $[(\ln I)_{exp} + \gamma]/(\pi/\sqrt{6}) = A$. Consider the ratio of the lognormal PDF of $\ln I$ evaluated at $(\ln I)_{LN}$ to the exponential PDF of $\ln I$ evaluated at $(\ln I)_{exp}$. The crossing of the two curves means that this ratio is $(\pi/\sqrt{6})/\sigma_{\ln I}$. Although the lognormal and exponential PDFs are used as an example, the same complicated interpretation of the graphs by Flatté et al. (1994) applies to all of their PDFs.

We simplify interpretation of our figures by graphing every PDF scaled by its respective simulation's value of σ, and the abscissa for every PDF is $(\ln I + 0.5\,\sigma^2)/\sigma$, where σ is the value from the respective simulation as defined in (29), and $\ln I$ is the value at the center of each final bin. Thus, if two curves coincide on our figures, then the two PDFs are equal at the same value of $\ln I$. In each figure, we choose the lognormal PDF to have the same value of $\sigma^2_{\ln I}$ as our simulation. Thus, on our figures, the lognormal is always the same curve and serves as a reference.

Figures 2a–c respectively show our cases for $\ell_0/R_F = 0$, 0.5, and 1.0 for our smallest value of Rytov variance, namely, 0.06. Only Beckmann's, the lognormal, and the simulations' PDFs are shown because the LNME and K PDFs do not exist for irradiance variance less that unity. One can see that the simulations' PDFs noticeably depart from the weak-scintillation asymptote of a lognormal PDF even for σ^2_{Rytov} as small as 0.06 and that Beckmann's PDF is in better agreement with the corresponding simulation's PDF than is the lognormal PDF. Increasing inner scale from Fig. 2a to Fig. 2c causes the PDFs to become closer to the lognormal PDF, even though the statistical moments change very little as ℓ_0/R_F changes. In interpreting these slight

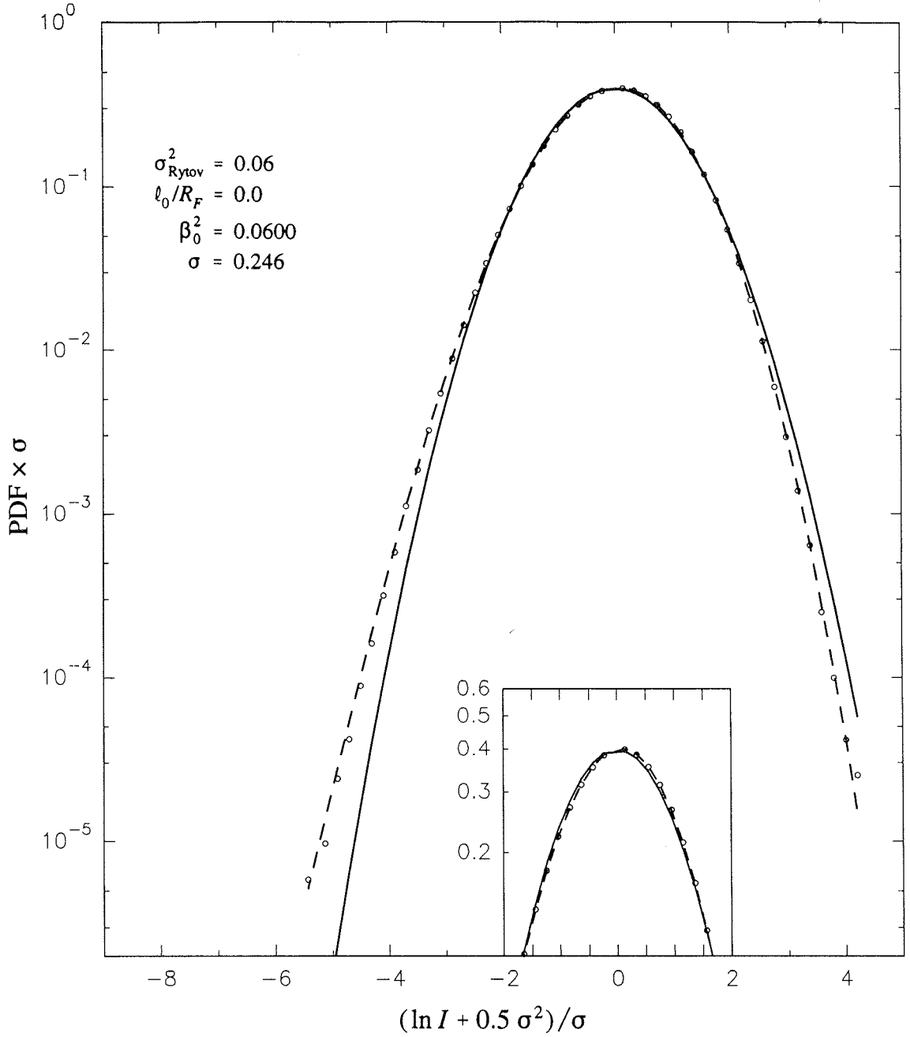

FIGURE 2a. PDF comparison.

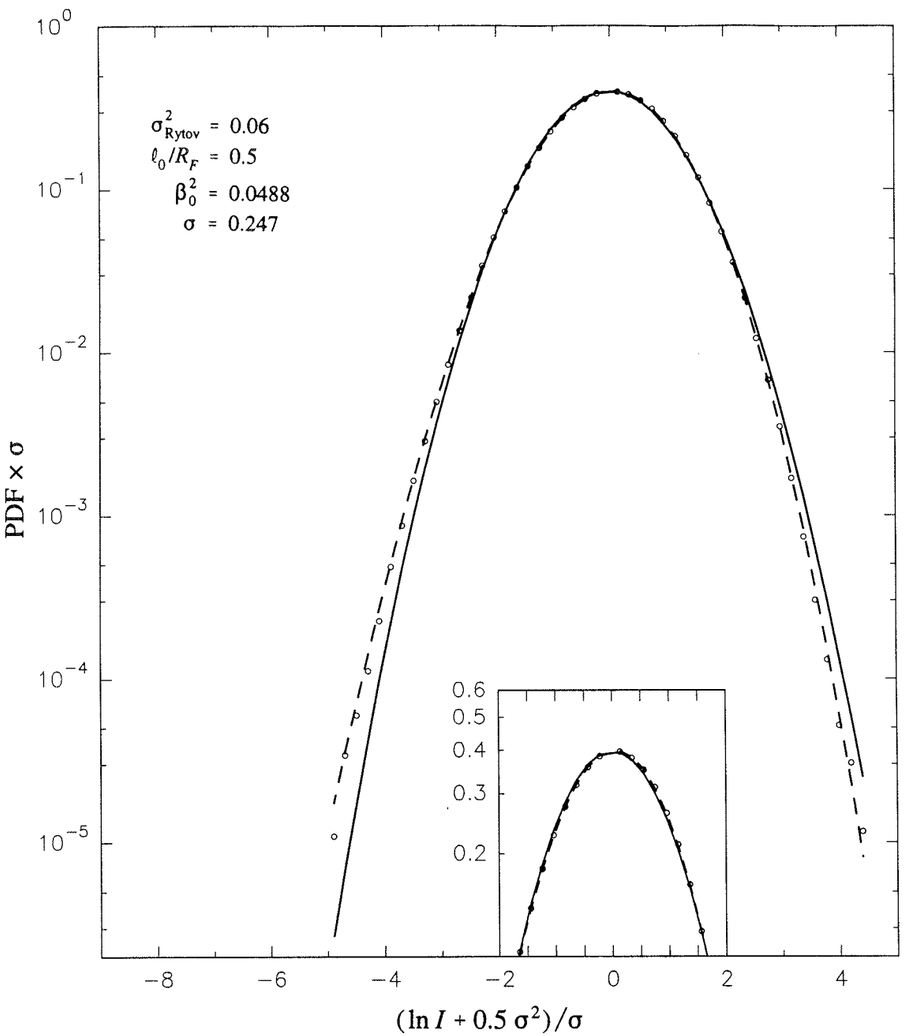

FIGURE 2b. PDF comparison.

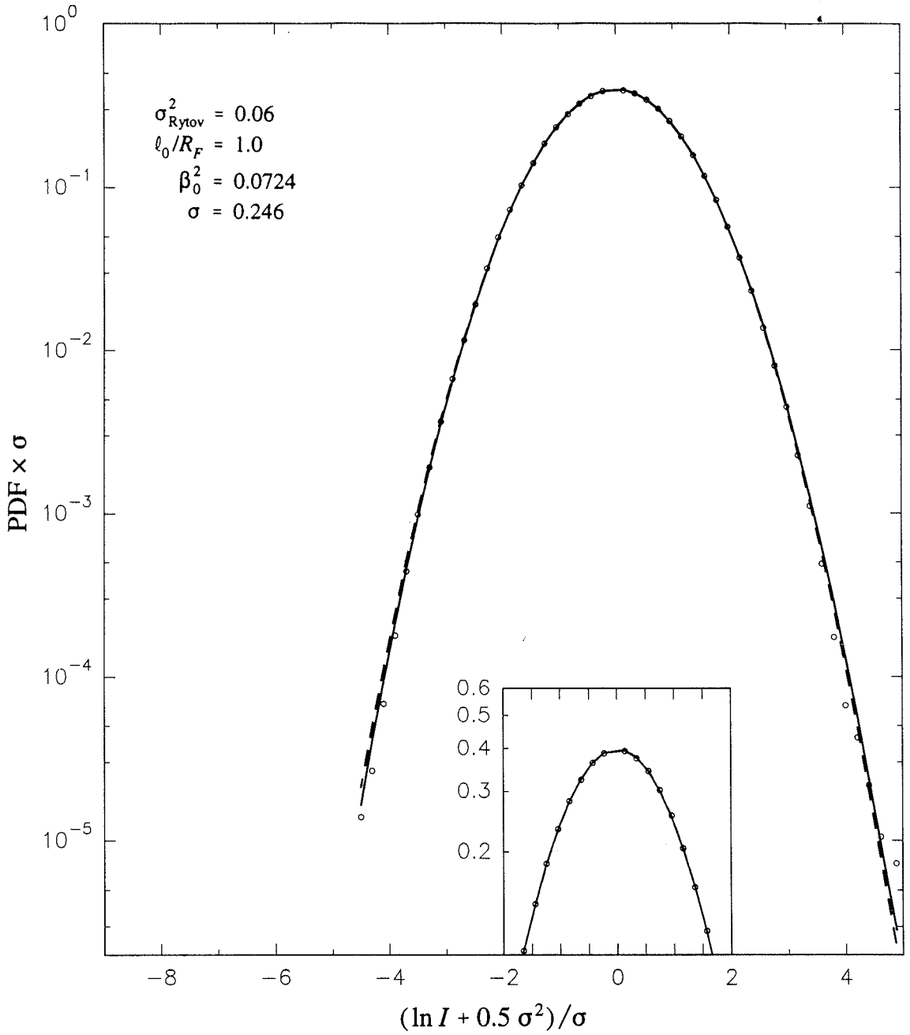

FIGURE 2c. PDF comparison.

changes, it must be kept in mind that the lognormal PDF is determined by the value of σ, whereas Beckmann's PDF is determined by the values of $<\ln I>$ and $<I^2>$.

Figures 3a–c show our three inner-scale cases for $\sigma^2_{Rytov} = 1.0$. The irradiance variance exceeds unity for these and all subsequent figures so that the K and LNME PDFs can be shown. The irradiance variance is so close to unity for Figs. 3a–c that the K and LNME PDFs are nearly equal to the exponential PDF, and the K and LNME PDFs are indistinguishable on the scale of the figures. Therefore, the K PDF is not shown on Figs. 3a–c. The simulations' PDFs are clearly in disagreement with the lognormal, K, and LNME PDFs in Figs. 3a–c and clearly in good agreement with Beckmann's PDF. An interesting feature of both the simulations' and Beckmann's PDFs is that on the left of the peak of the curves these PDFs appear to approach a straight line as log-irradiance decreases. This feature is most pronounced for $\ell_0/R_F = 1.0$ in Fig. 3c.

Figures 4a–c show our three inner-scale cases for $\sigma^2_{Rytov} = 2.0$. The LNME PDF is not shown on these figures because it is indistinguishable from Beckmann's PDF on the scale of Figs. 3a,b and would be just distinguishable on Fig. 3c with the deviations of the LNME PDF from Beckmann's PDF being in the direction toward the K PDF. That is, for $\sigma^2_{Rytov} = 2.0$, Beckmann's PDF has nearly approached its limiting behavior of becoming the LNME PDF. Beckmann's PDF is clearly the closest to the simulations' PDFs in Figs. 4a–c, and the LNME PDF is then also close to the simulations' PDFs. The greatest deviation of Beckmann's PDF and the simulations' PDFs is for the case of largest inner scale in Fig. 4c.

Figures 5a–c show our three inner-scale cases for $\sigma^2_{Rytov} = 5.0$. The LNME PDF is not shown in Fig. 5a because it is indistinguishable from Beckmann's PDF. Beckmann's PDF is not shown in Figs. 5b,c because fitting its parameters r and σ_z^2 failed for all combinations of statistics that we tried. In fact, for the case in Fig. 5a, we obtained r and σ_z^2 from $<I^{-1/2}>$ and $<I^2>$ because we failed to obtain these parameters from $<\ln I>$, $<I^2>$, or any other statistics that we tried. Essentially, Beckmann's PDF must be forced to be the LNME PDF for cases of such large irradiance variance. In Figs. 5a–c, we see that the LNME PDF (same as Beckmann's PDF in Fig. 5a) progressively departs from the simulations' PDFs as ℓ_0/R_F increases (and therefore as irradiance variance increases since σ^2_{Rytov} is fixed), although qualitative agreement remains. The K and lognormal PDFs are significantly different from the simulations' PDFs in Figs. 5a–c. The K PDF fits the simulations' PDFs well on the extreme right-hand sides of Figs. 5a–c and is, in fact, superior to the fit of the LNME PDF in places. Because of the great difference between the K PDF and simulations' PDFs on the left-hand side of Figs. 5a–c, we see that if a statistic that emphasizes small values of log-irradiance is used instead of $<I^2>$ to determine the parameter of the K PDF, then the K PDF would disagree substantially on the extreme right-hand sides of Figs. 5a–c.

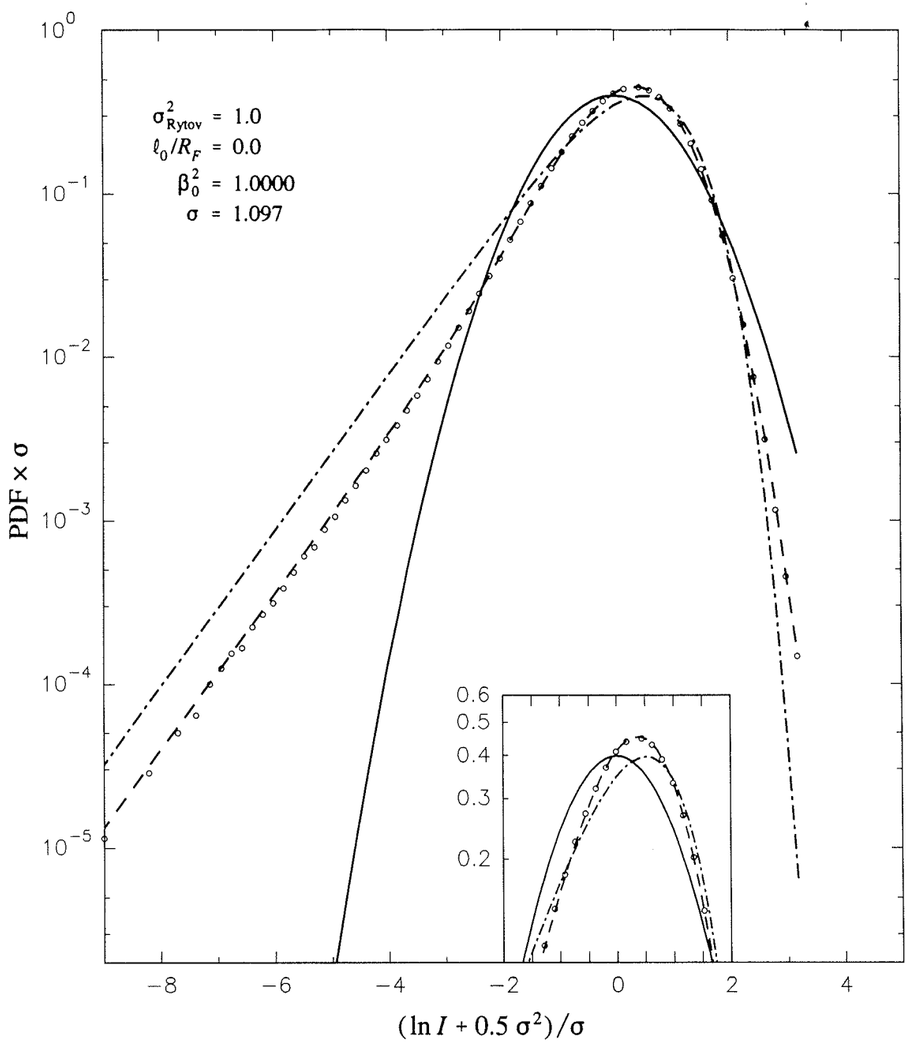

FIGURE 3a. PDF comparison.

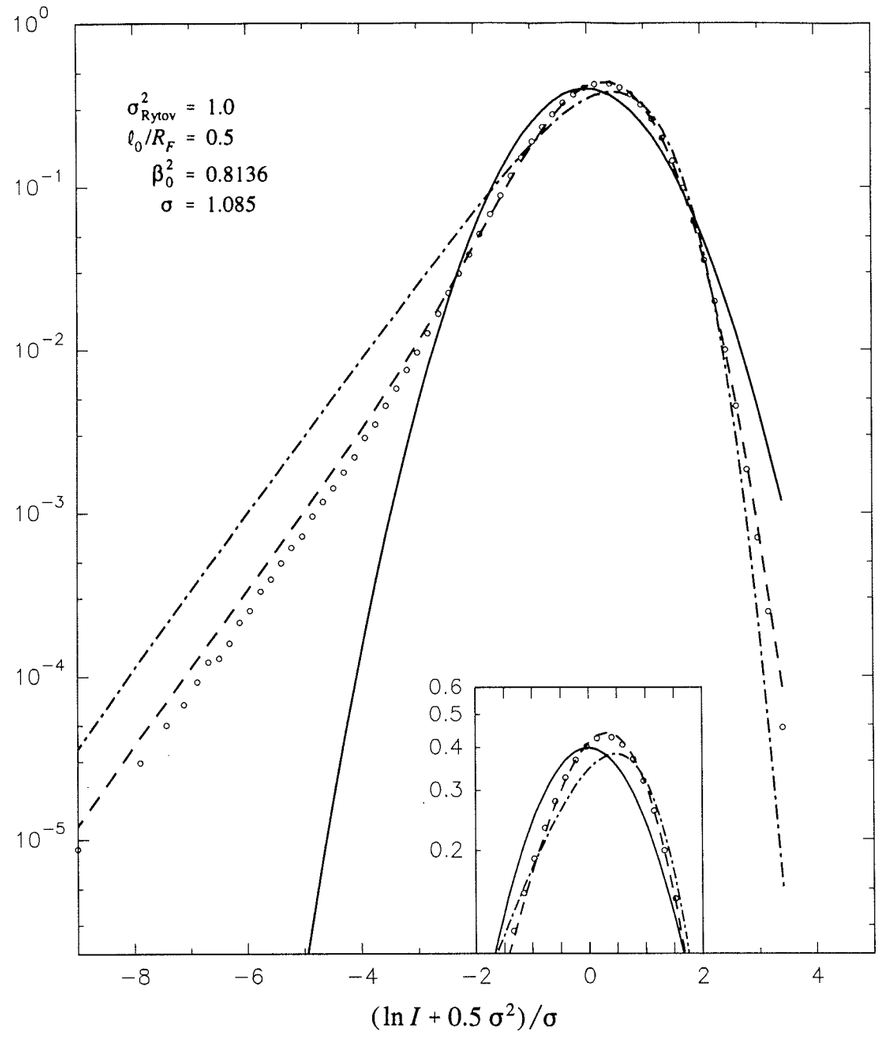

FIGURE 3b. PDF comparison.

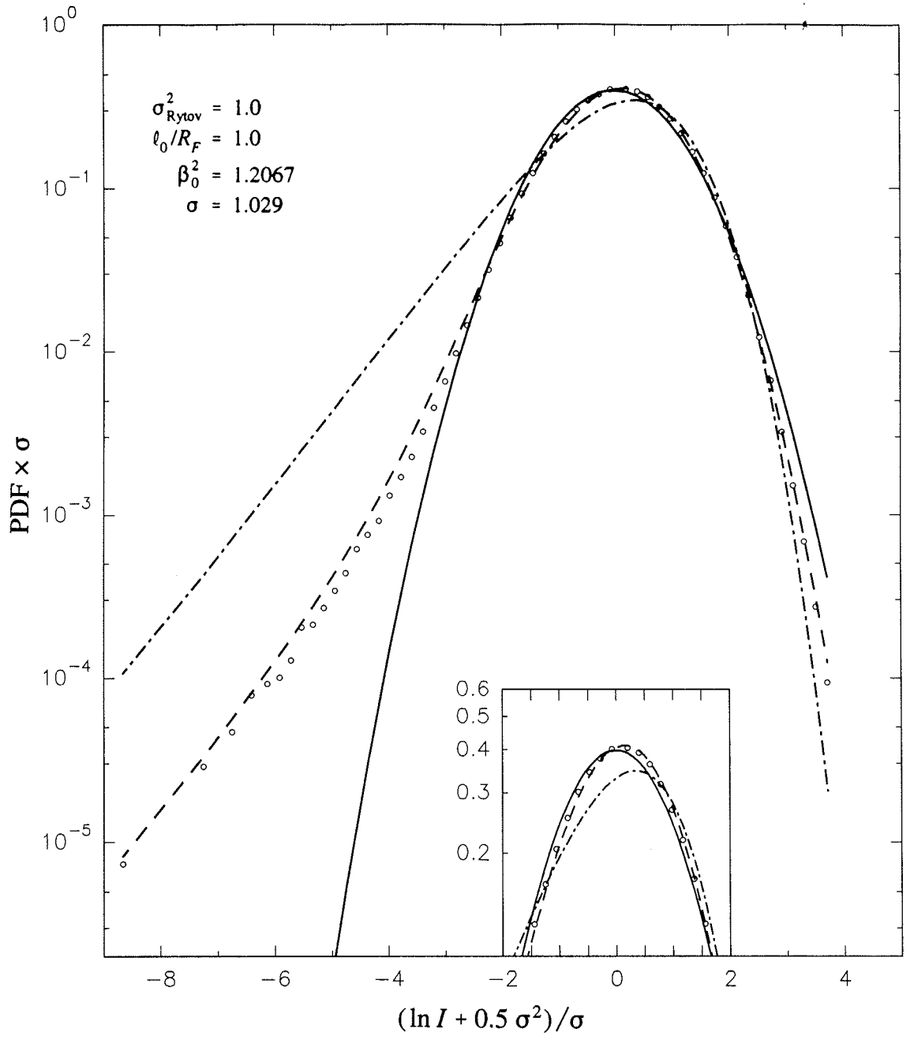

FIGURE 3c. PDF comparison.

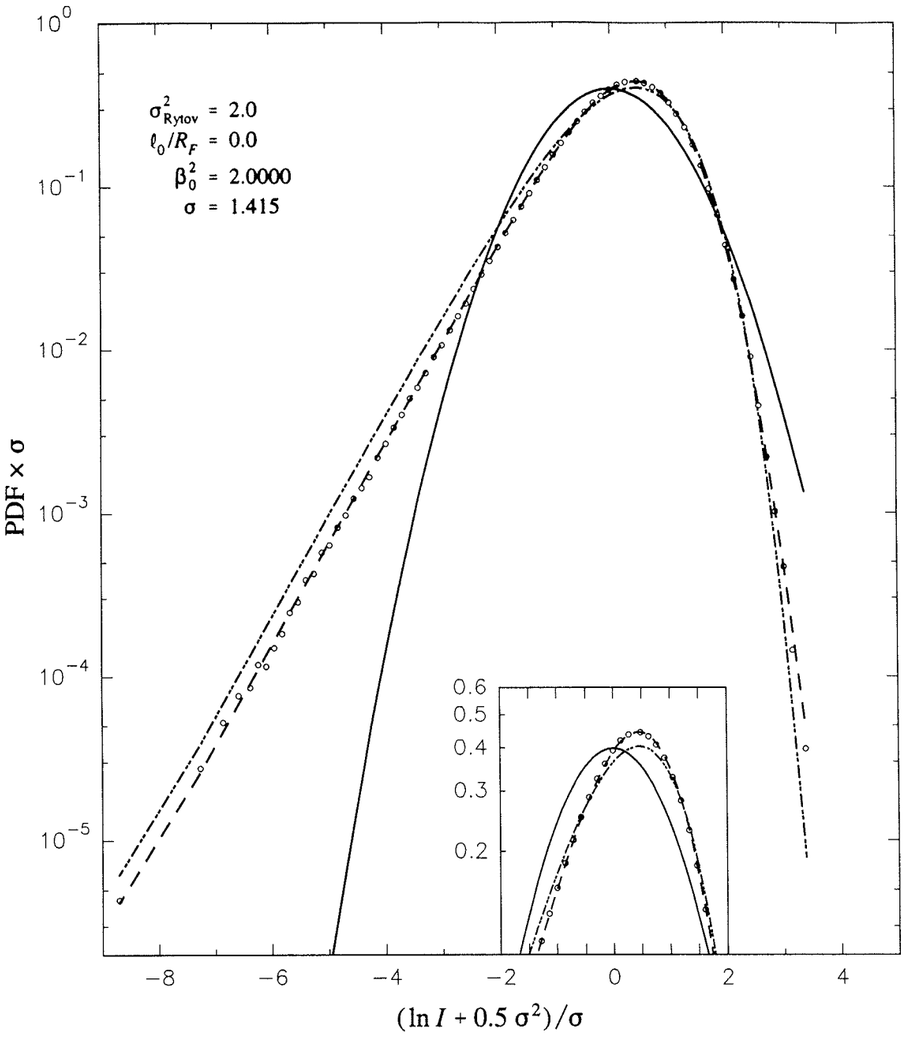

FIGURE 4a. PDF comparison.

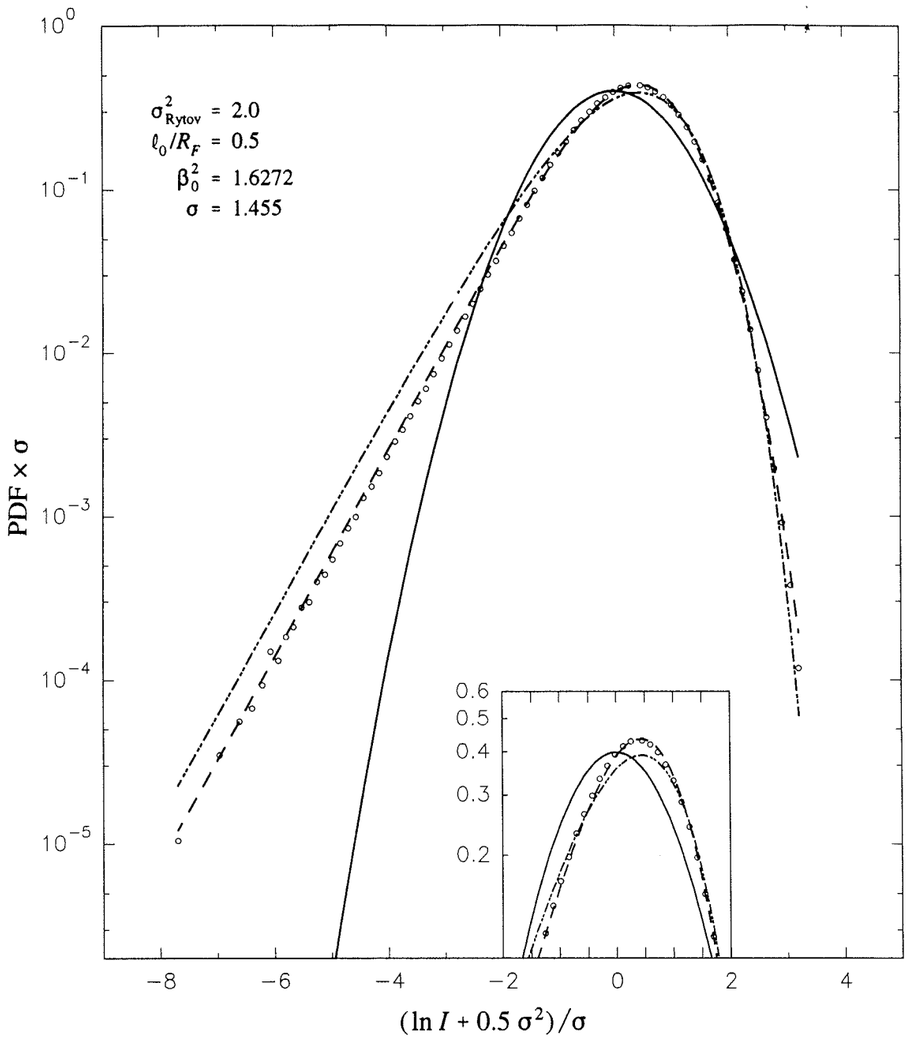

FIGURE 4b. PDF comparison.

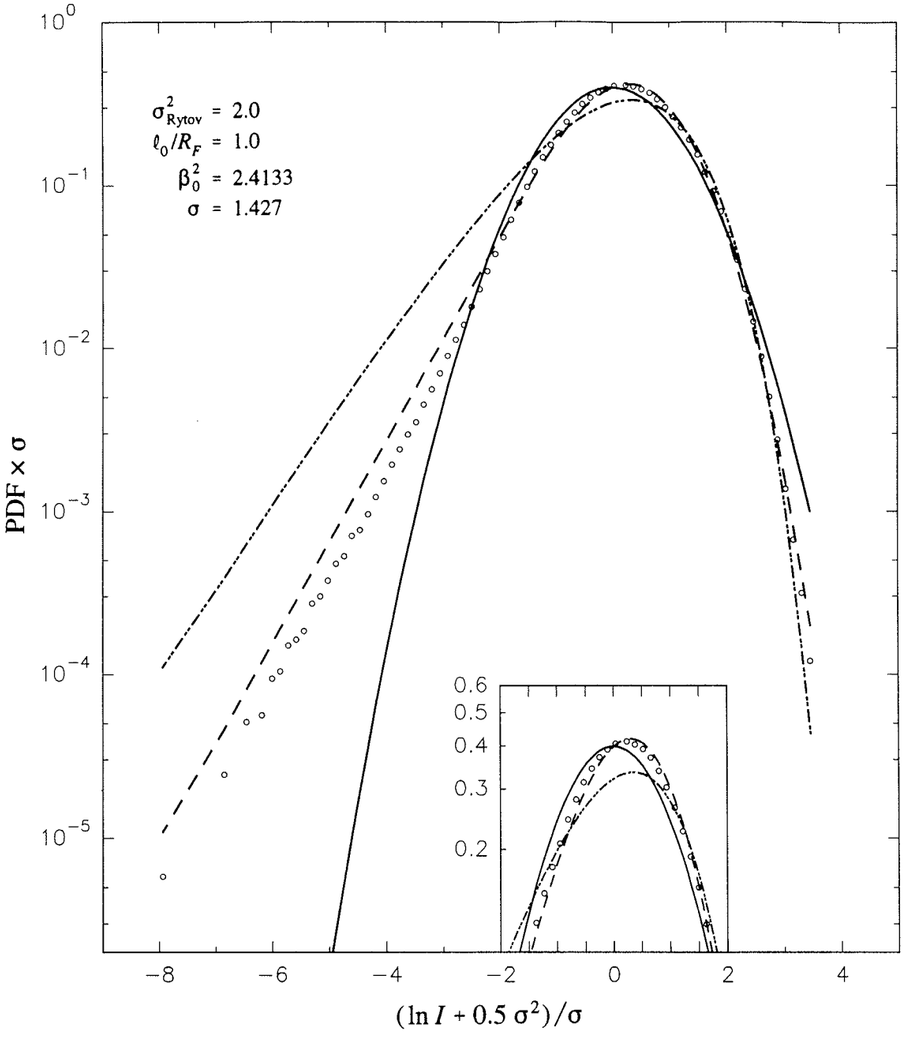

FIGURE 4c. PDF comparison.

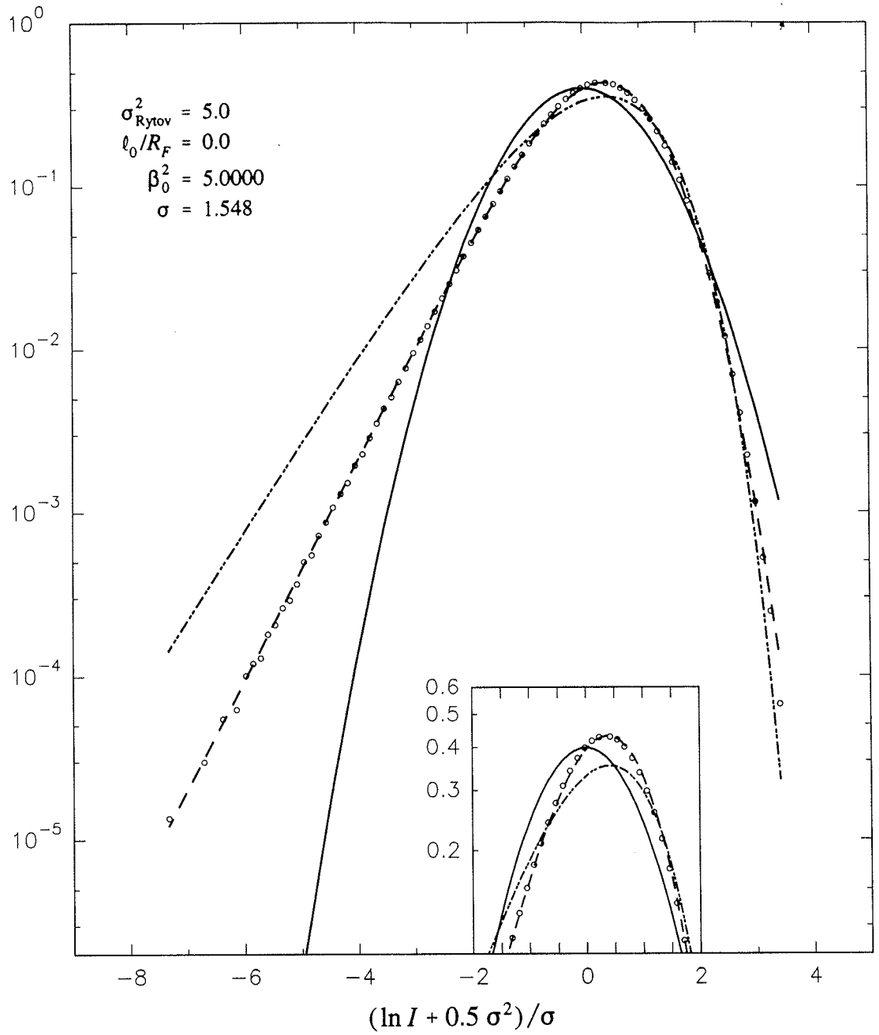

FIGURE 5a. PDF comparison.

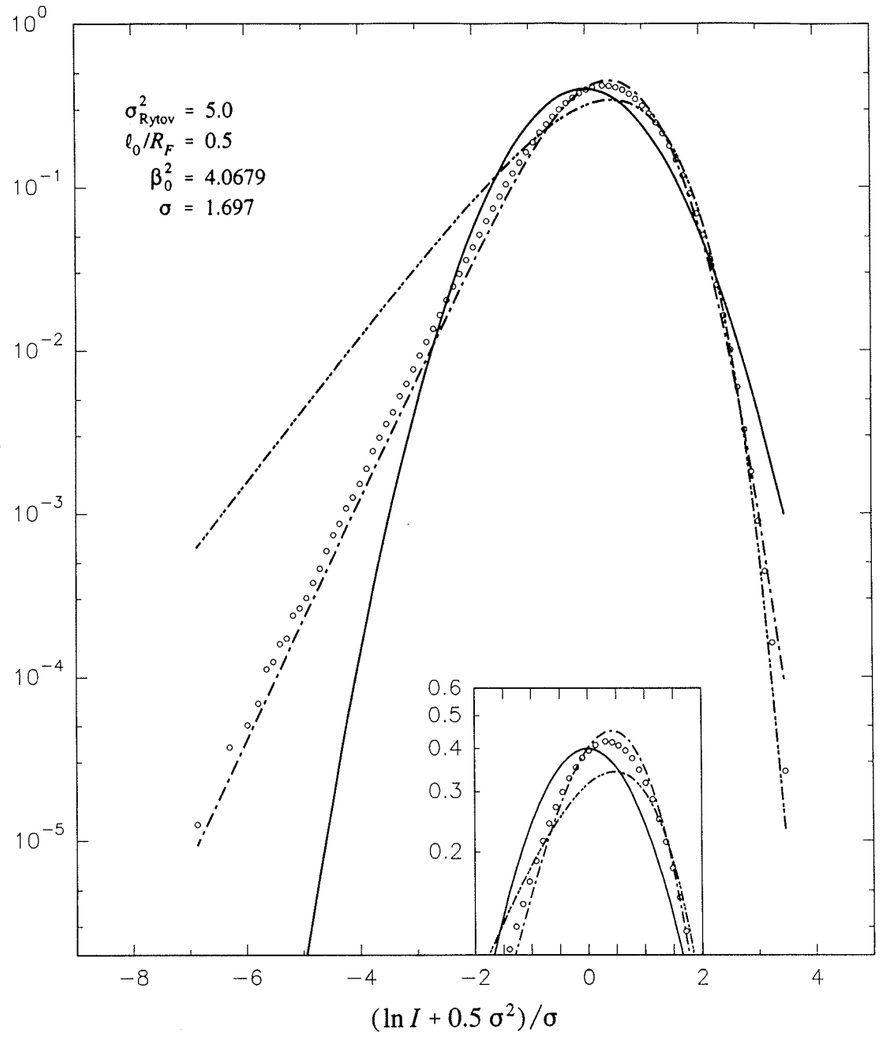

FIGURE 5b. PDF comparison.

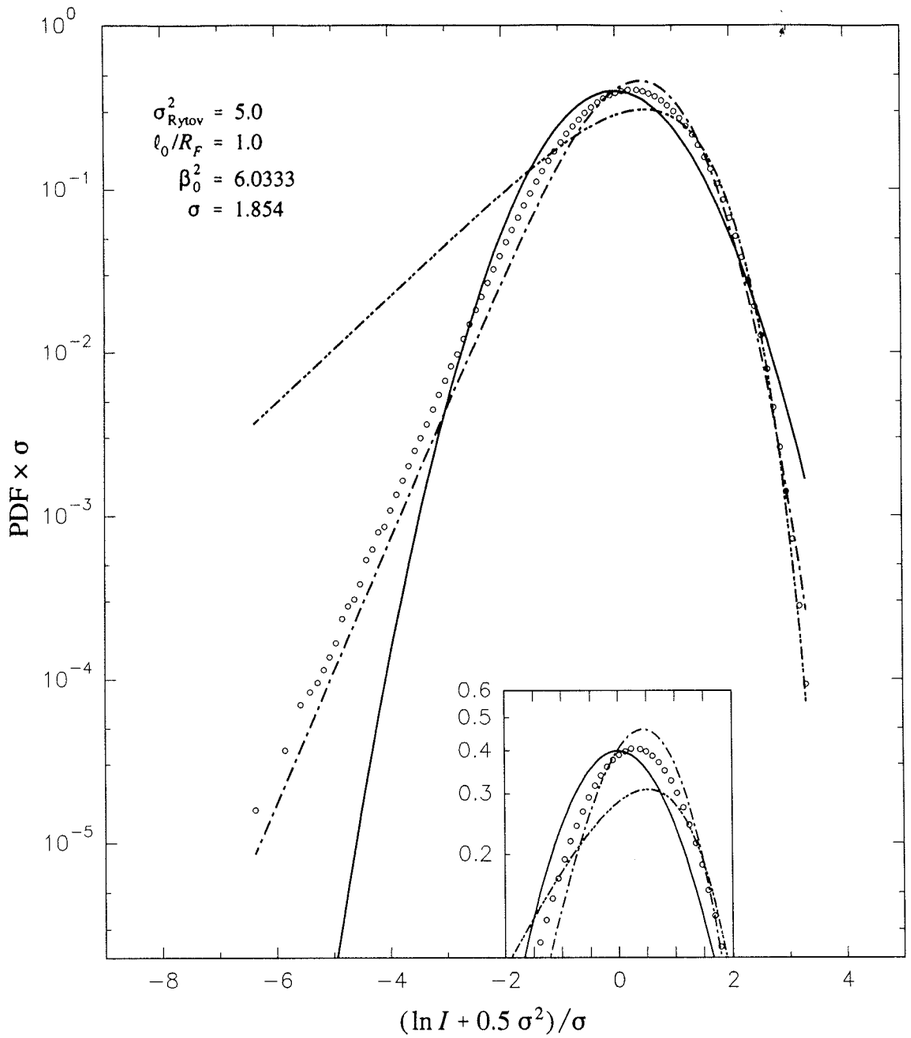

FIGURE 5c. PDF comparison.

7. STATISTICS CALCULATED FROM SIMULATIONS

Before presenting tabulations of various statistics, we show the corresponding integrands to demonstrate the accuracy of the statistics. Given a function $f(\ln I)$ of $\ln I$, the average of f is given by the integral of f multiplied by the PDF of $\ln I$, that is,

$$\langle f(\ln I)\rangle = \int_{-\infty}^{\infty} d\ln I \; f(\ln I)\; \mathrm{PDF}(\ln I)\ . \tag{32}$$

We present the integrands $f(\ln I)\ \mathrm{PDF}(\ln I)$ for $f = \ln I$, $(\ln I - \langle \ln I\rangle)^2$, $I^{-1/2}$, I^2, and I^3 for our cases of largest variance. These cases of large variance can cause the integral (32) on a finite interval to underestimate the statistic. Cases for which all PDFs have accurate values of a given statistic are not shown in the figures. Each simulation's PDF was calculated using 2000 bins equally spaced in $\ln I$ from -15 to 5. The simulation's integrands are shown as solid line segments connecting the centers of these 2000 bins. The heuristic model PDFs were also calculated at each of these bin centers, and their statistics were calculated by numerical integration over the 2000 bins from -15 to 5. Of course, the statistics from each simulation were also calculated in this manner. Although many statistics of the heuristic PDFs can be obtained from analytic formulas, we have not done so. These analytic formulas are well known and can be applied as desired.

Figures 6a–c show the integrands for $f = \ln I$ and the case of largest σ^2_{Rytov}. Only the K PDF fails to converge on the left side of Fig. 6c, indicating that the value of $\langle \ln I\rangle$ from the K PDF is somewhat underestimated for that case. Figures 7a–c show the integrands for $f = (\ln I - \langle \ln I\rangle)^2$. Again, there are two cases for which the K PDF will give an underestimated value of $\sigma^2_{\ln I}$, but the other PDFs will give correct values. In Figs. 8a–c, the integrands for $f = I^{-1/2}$ are shown for $\sigma^2_{Rytov} = 5.0$, and Fig. 8d shows the case $\sigma^2_{Rytov} = 2.0$. Again, the K PDF will have underestimated values of $\langle I^{-1/2}\rangle$ calculated by the numerical integration, whereas the other PDFs will have correct values. Figures 9a–c show the second-moment integrand, i.e., $f = I^2$, for $\sigma^2_{Rytov} = 5.0$, and Figs. 9d–f show it for $\sigma^2_{Rytov} = 2.0$. The lognormal PDF has its second moment underestimated in all these cases, as does the LNME PDF for Figs. 9a,b, and to a much lesser extent for the LNME and Beckmann's PDFs for Figs. 9a and 9f. Figures 10a–f show the third-moment integrand, i.e., for $f = I^3$. The third moment is seen to be underestimated in most cases, the exceptions being K PDF in all of Figs. 10a–f and the LNME and Beckmann's PDFs in Figs. 10d,e. The simulations' integrands for $f = I^3$ show great variability and lack of convergence to the abscissa, which indicates that the third moments obtained from the simulations are underestimated and have significant random error because there are too few events in the simulations to adequately determine the third moment of irradiance for the cases in these figures.

Table 4 gives the statistics obtained by numerical integration of the PDFs, including many footnotes to explain the entries. The simulations' statistics are accompanied by an error value if the error was calculated during the simulations' computer runs. This error is obtained by calculating the statistic from each realization and calculating the standard deviation of the

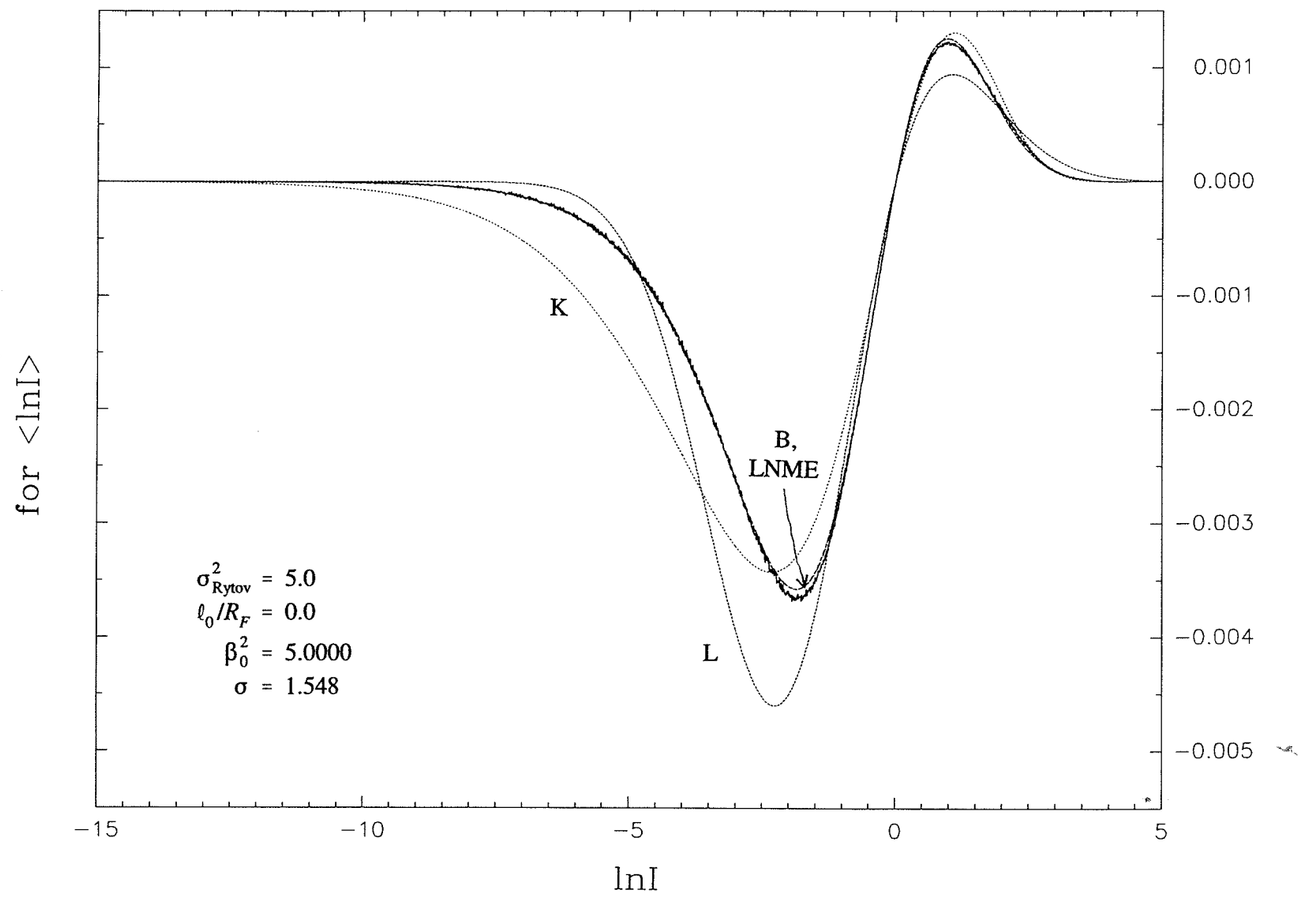

FIGURE 6a. Integrands for $f = \ln I$.

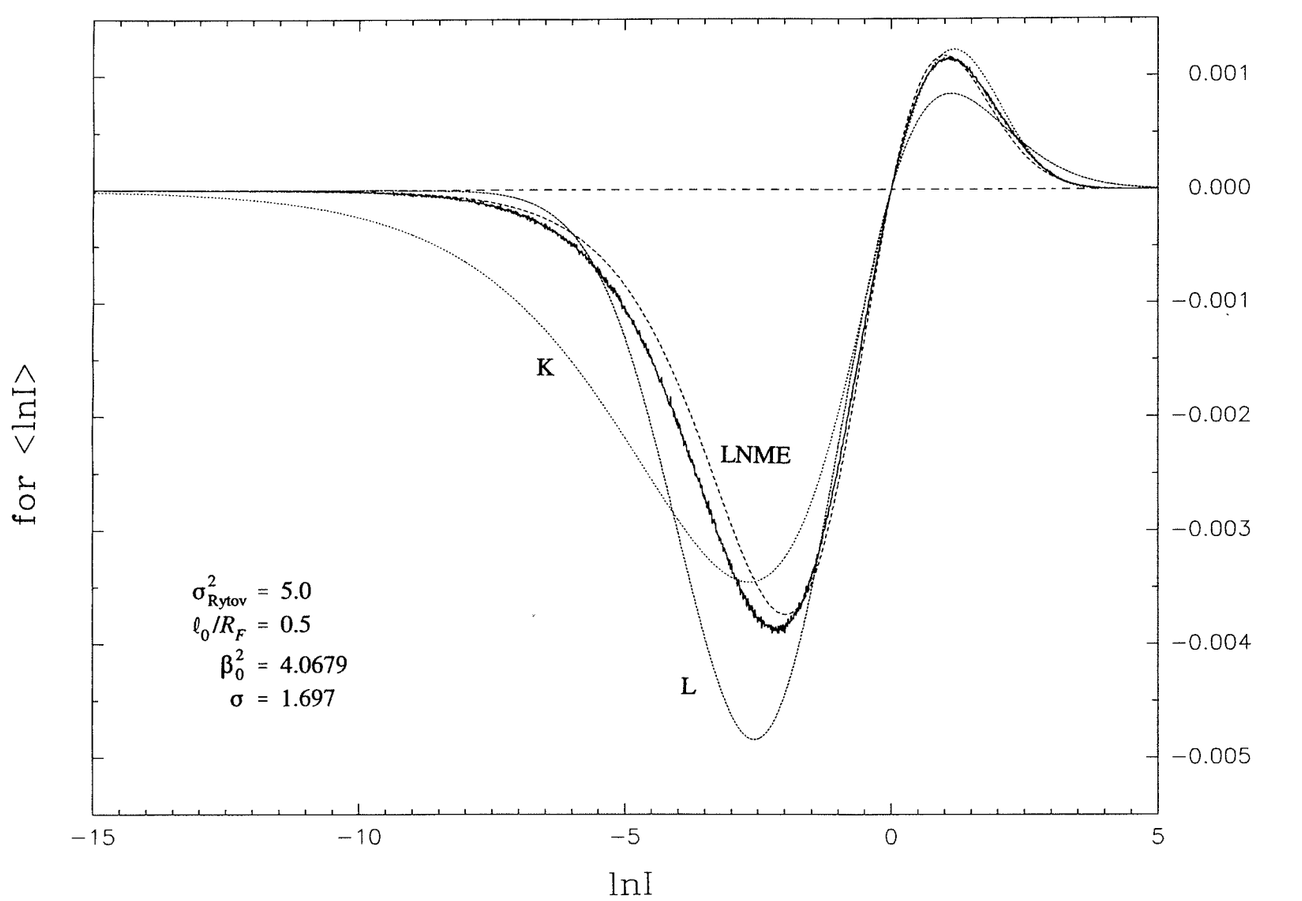

FIGURE 6b. Integrands for $f = \ln I$.

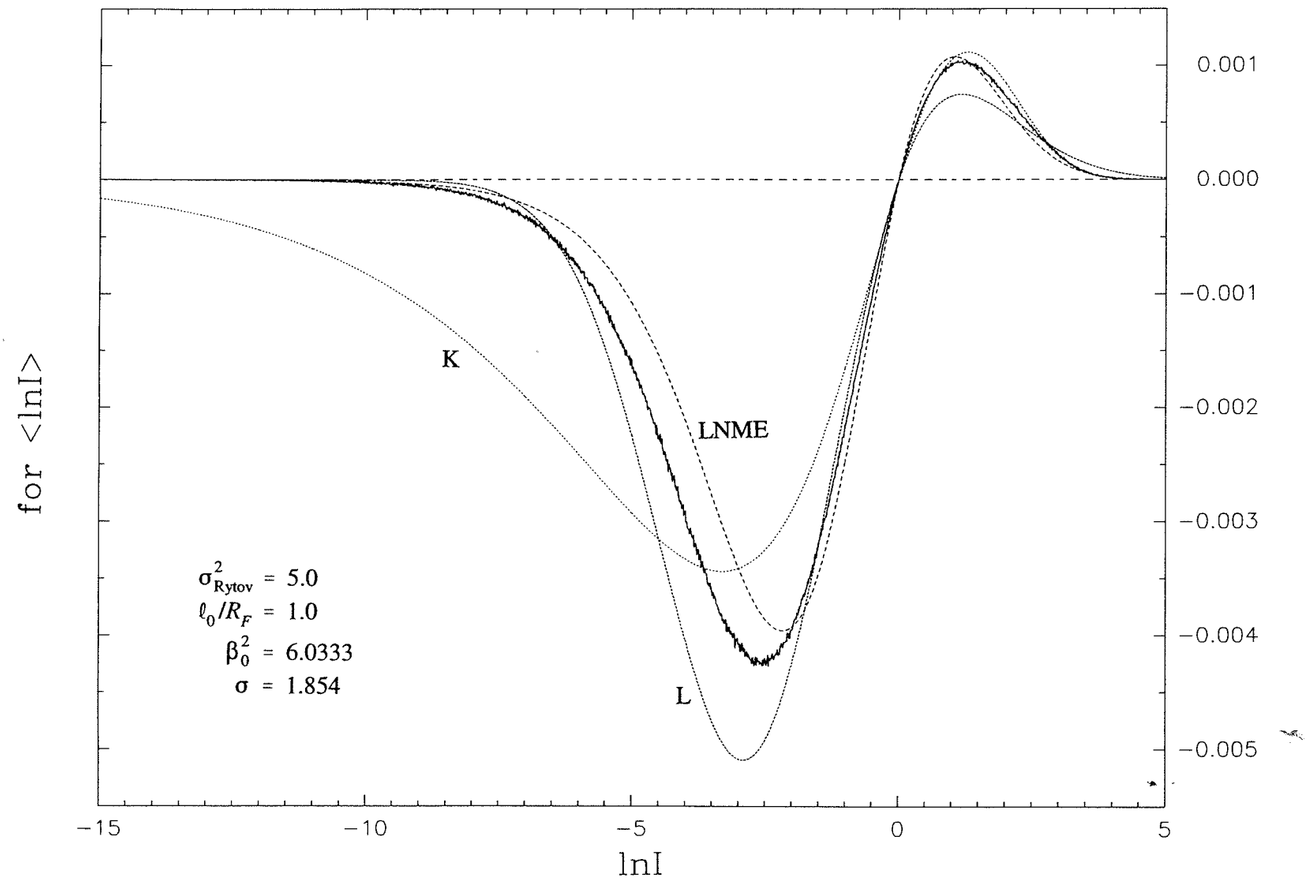

FIGURE 6c. Integrands for $f = \ln I$.

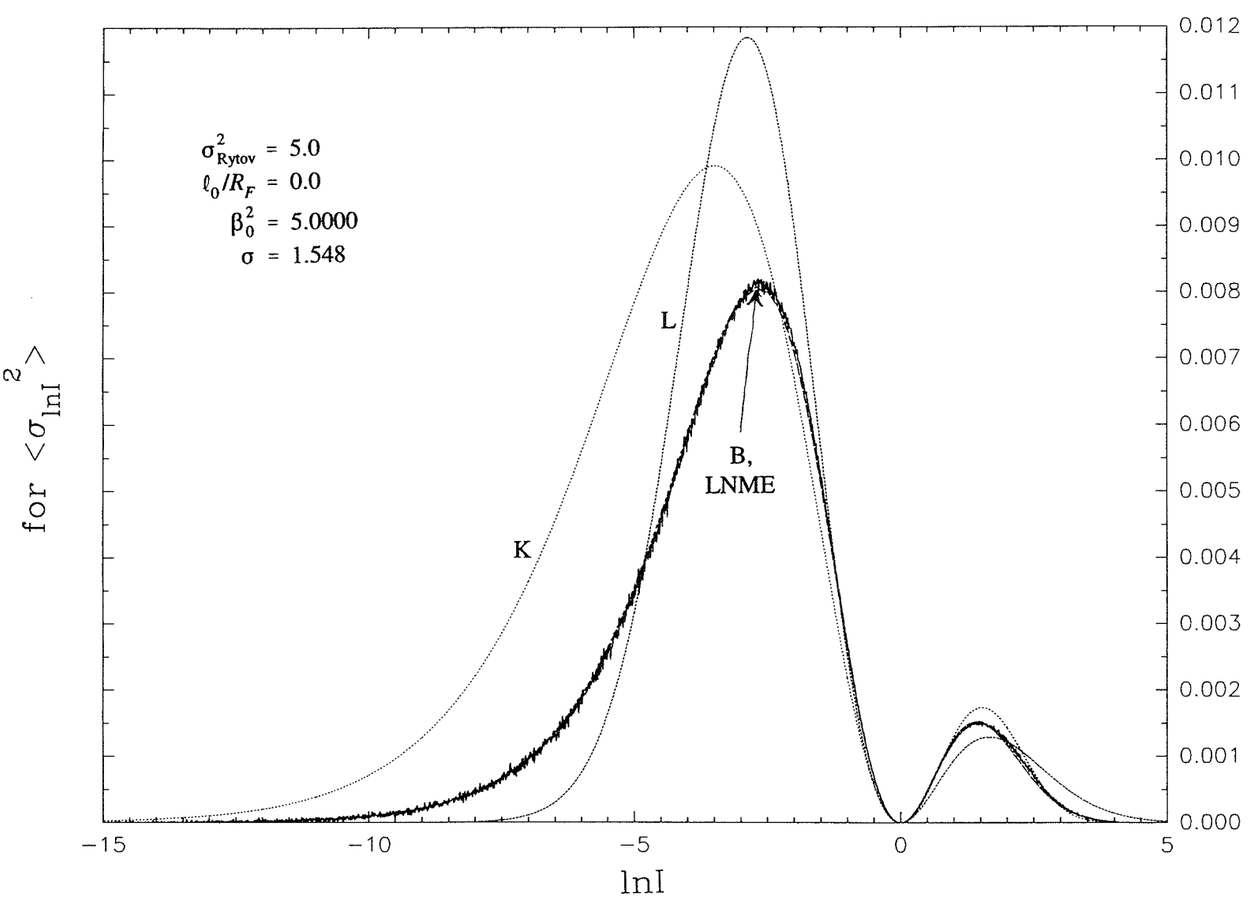

FIGURE 7a. Integrands for $f = (\ln I - <\ln I>)^2$.

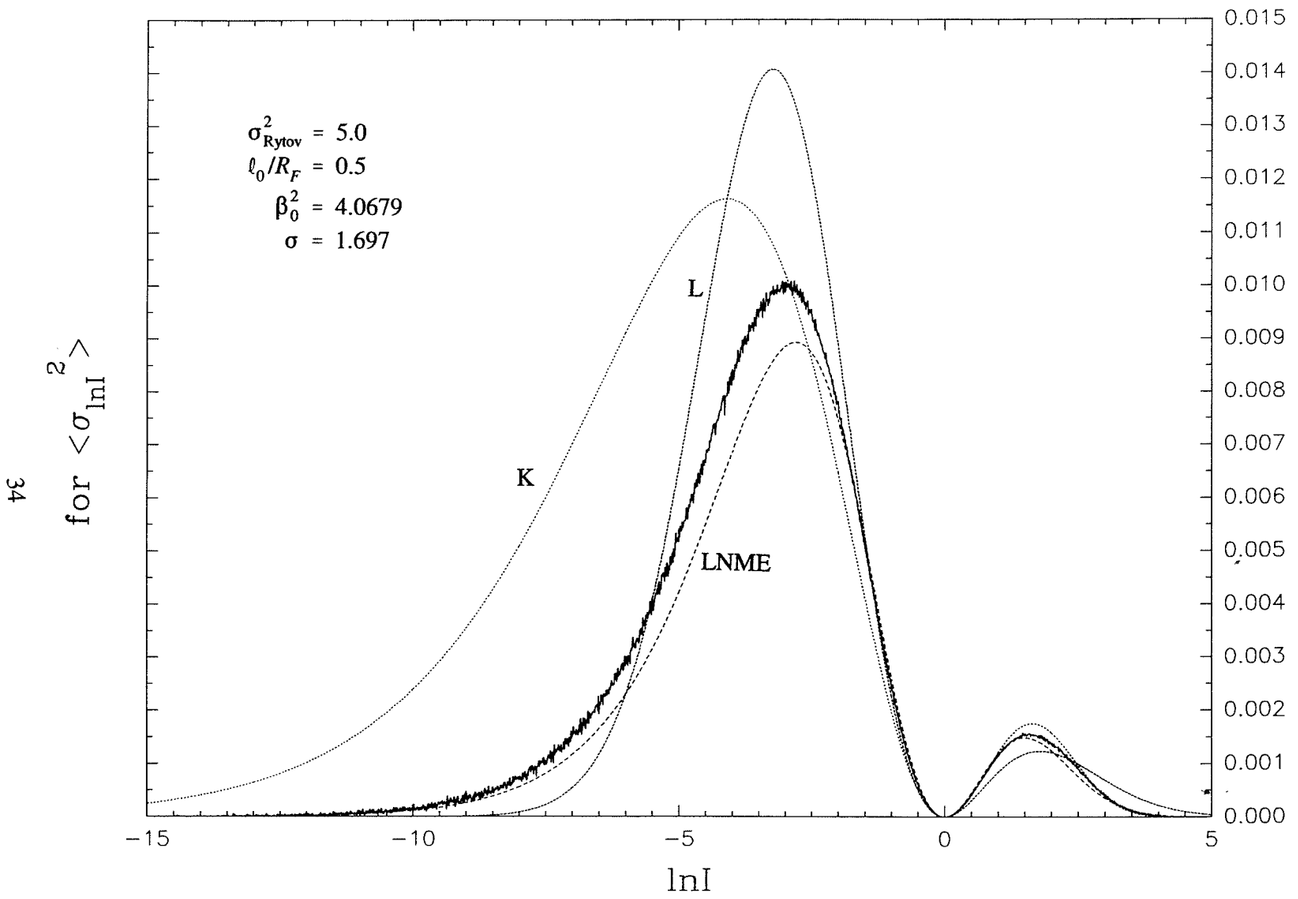

FIGURE 7b. Integrands for $f = (\ln I - <\ln I>)^2$.

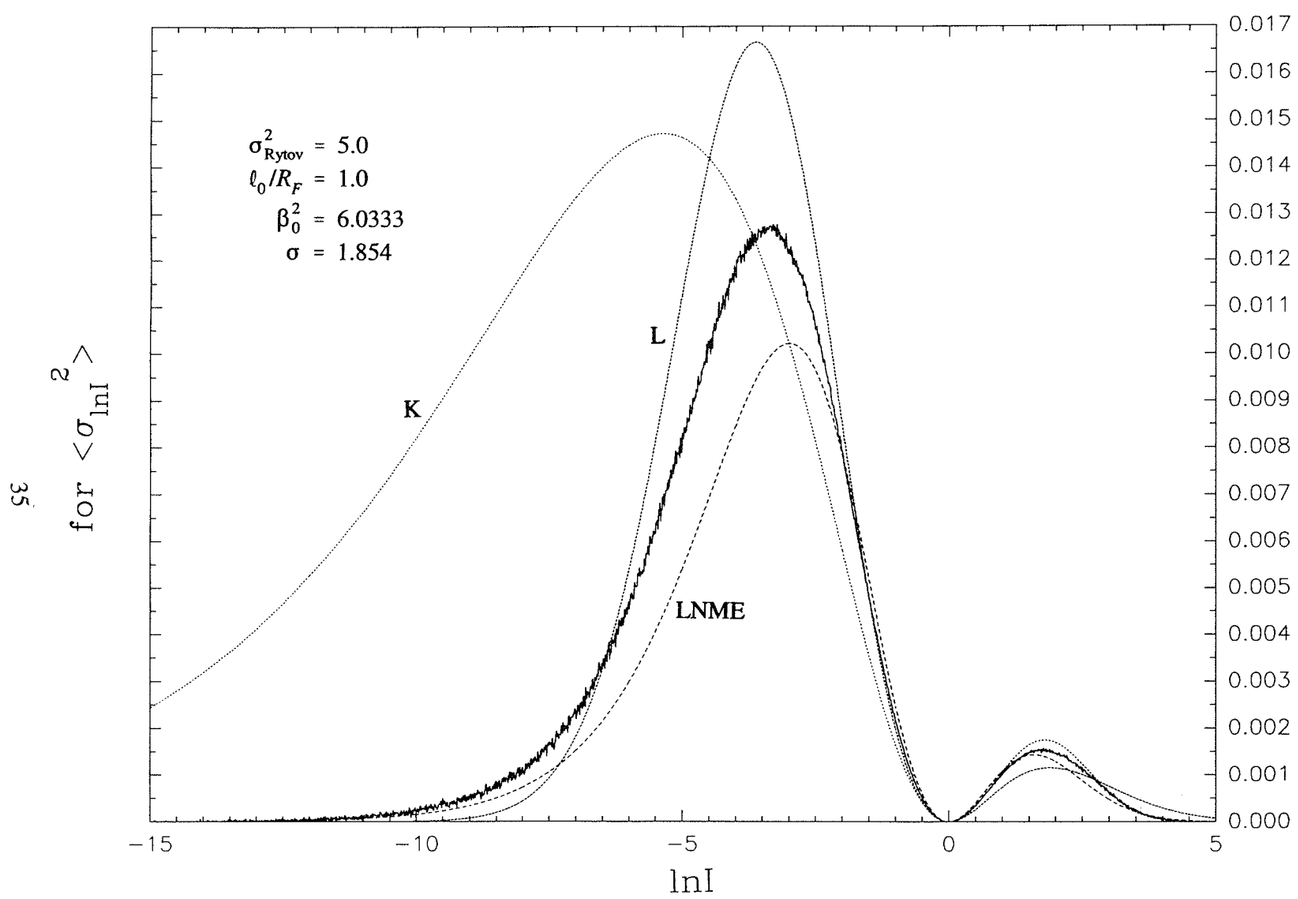

FIGURE 7c. Integrands for $f = (\ln I - <\ln I>)^2$.

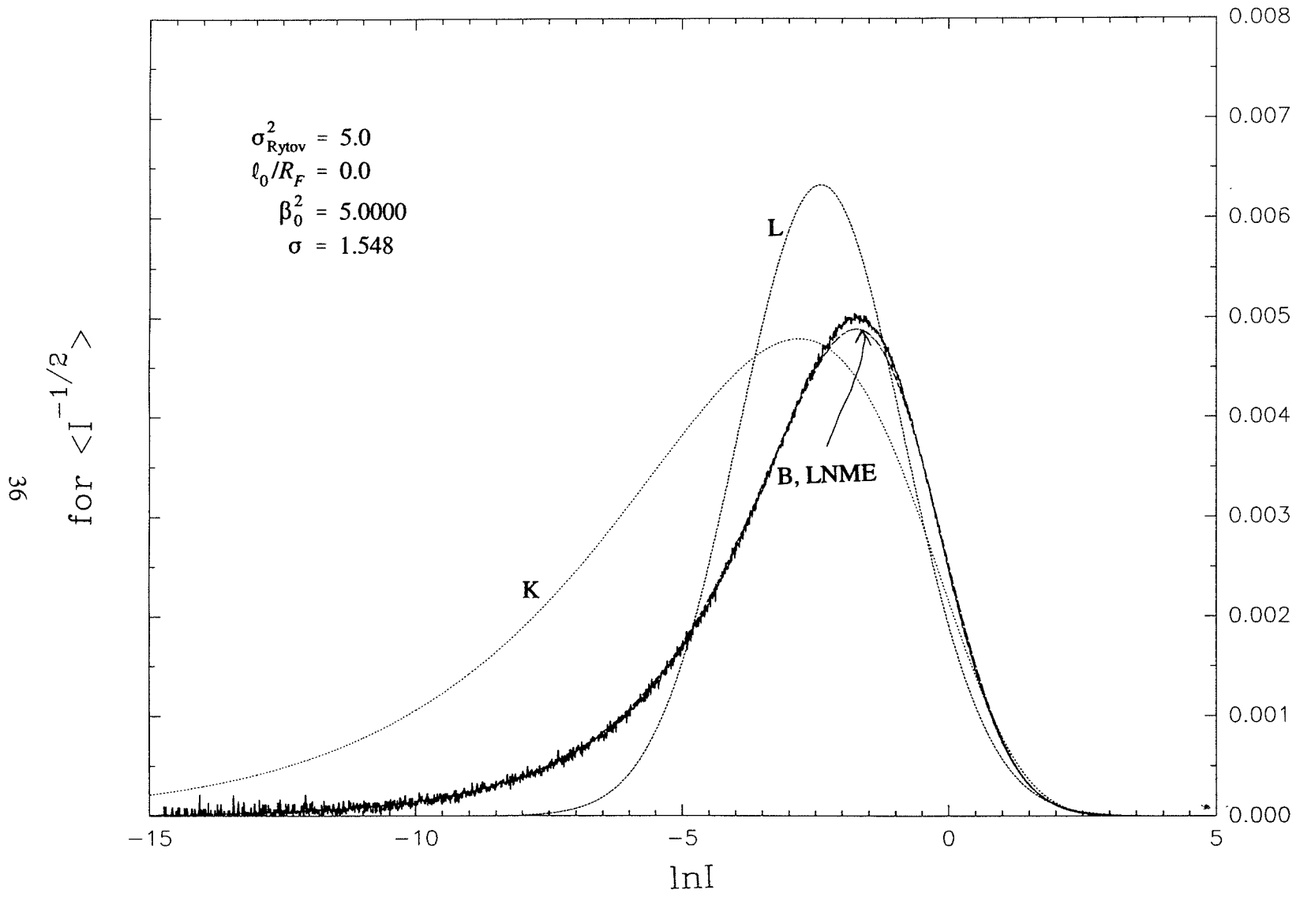

FIGURE 8a. Integrands for $f = I^{-1/2}$.

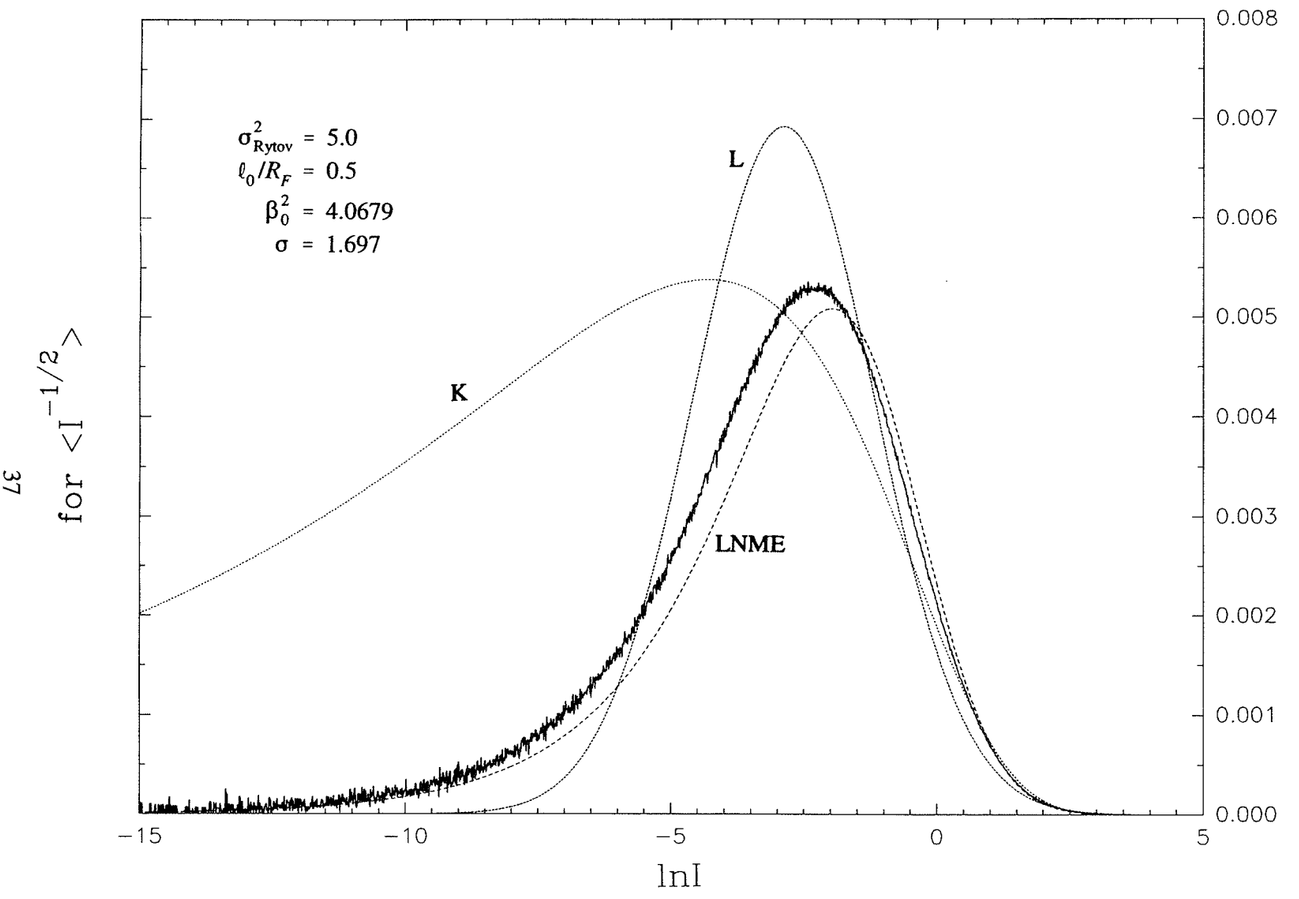

FIGURE 8b. Integrands for $f = I^{-1/2}$.

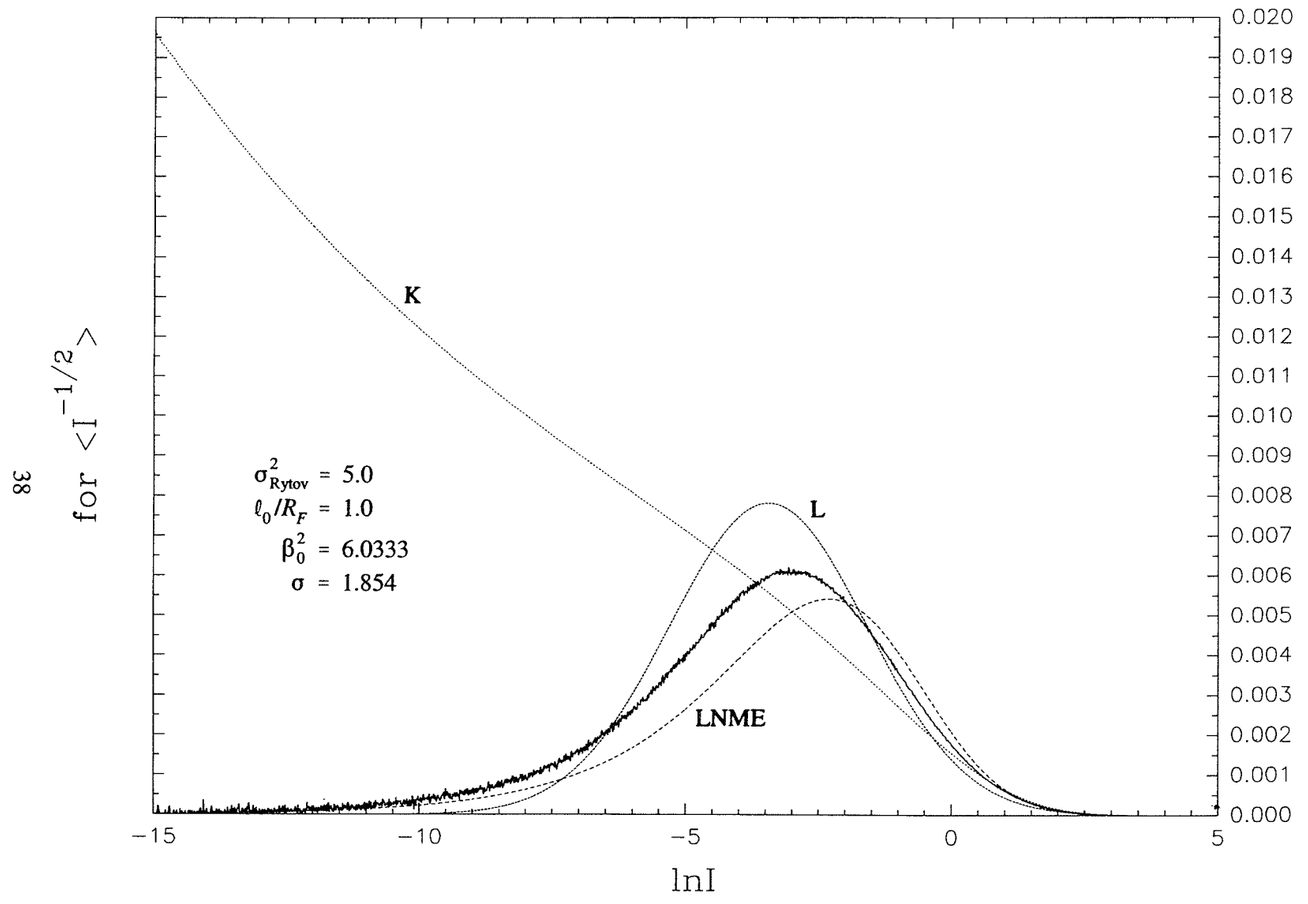

FIGURE 8c. Integrands for $f = I^{-1/2}$.

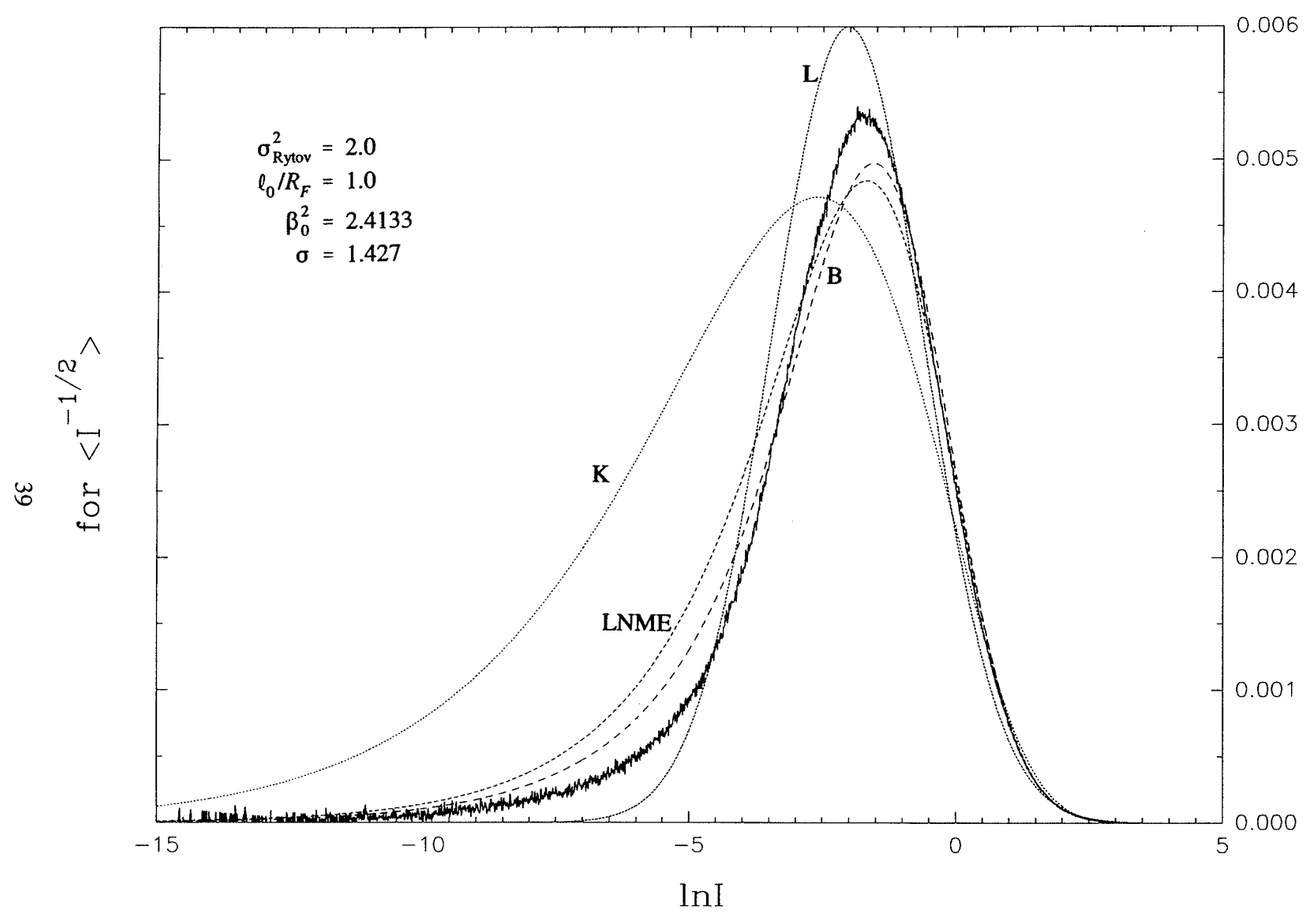

FIGURE 8d. Integrands for $f = I^{-1/2}$.

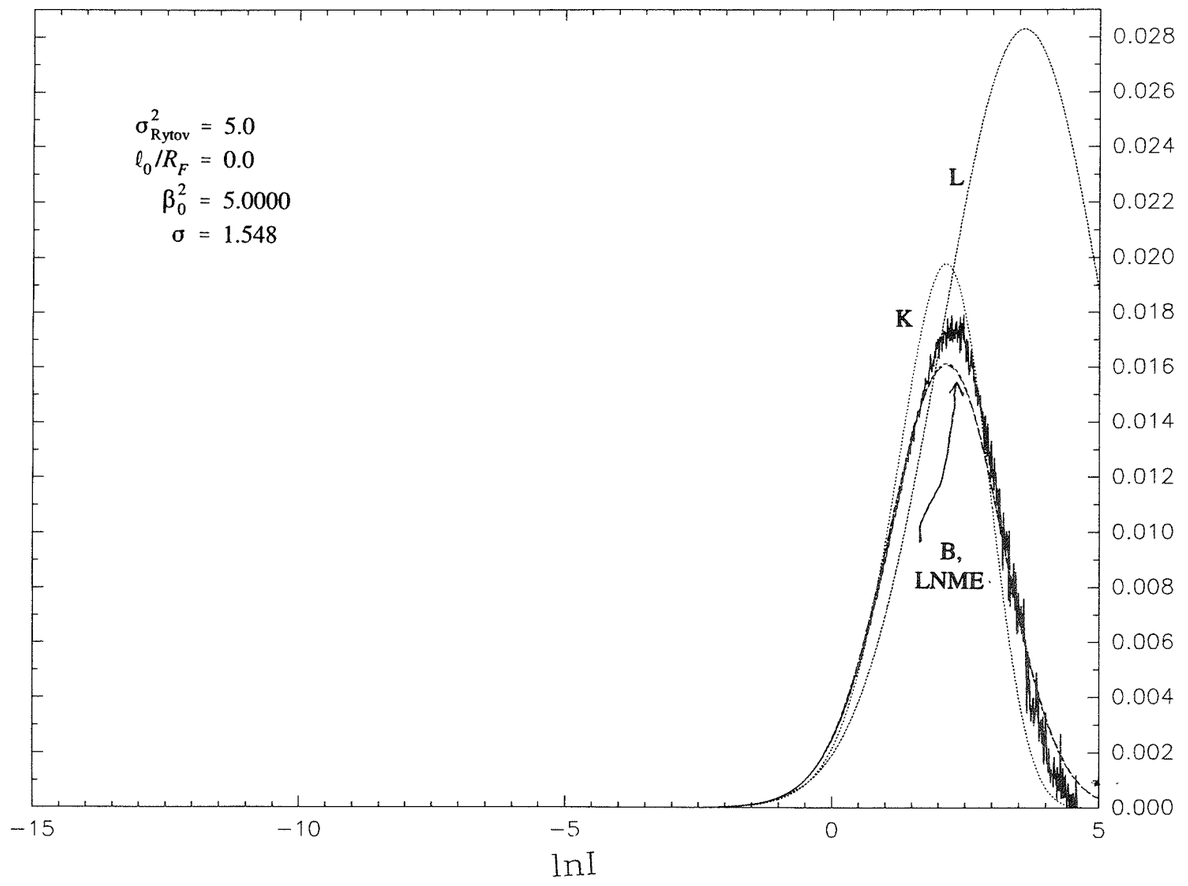

FIGURE 9a. Integrands for $f = I^2$.

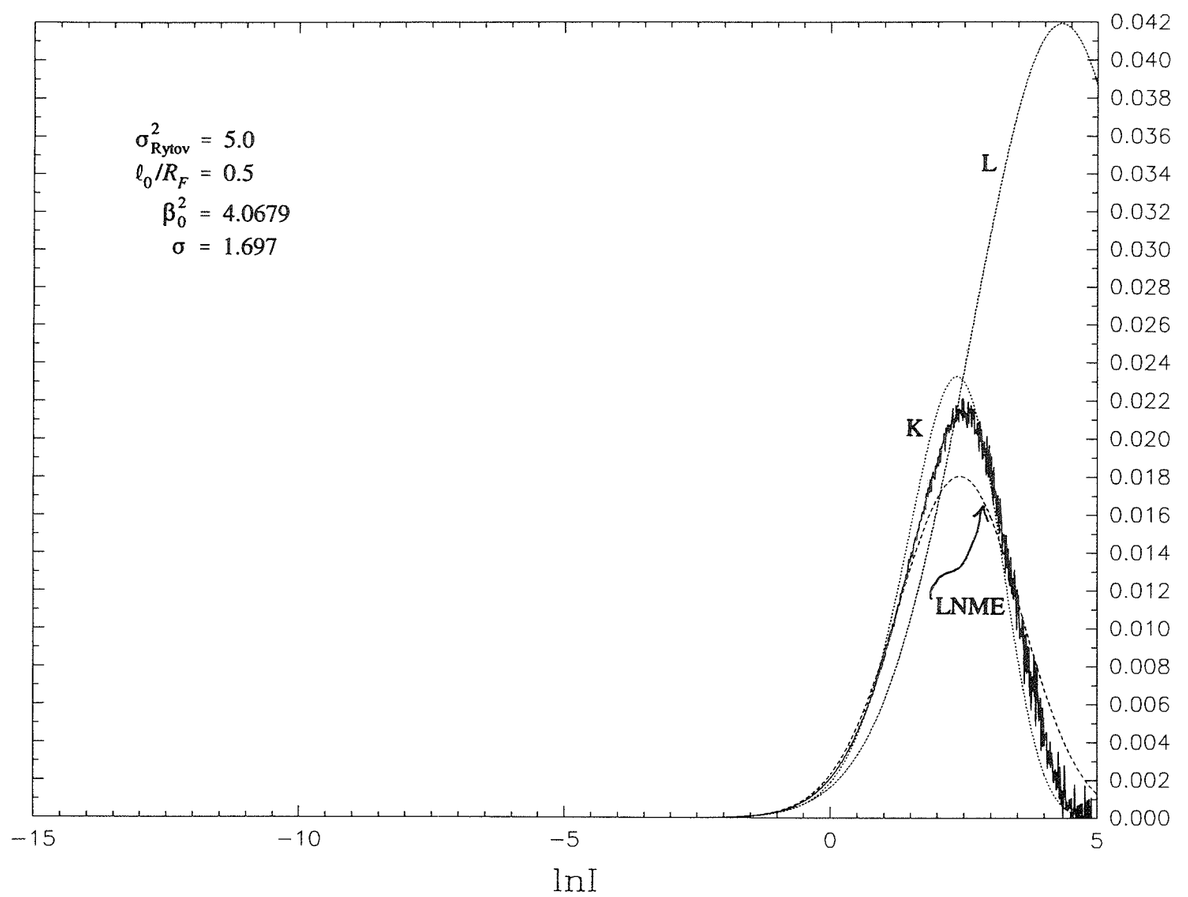

FIGURE 9b. Integrands for $f = I^2$.

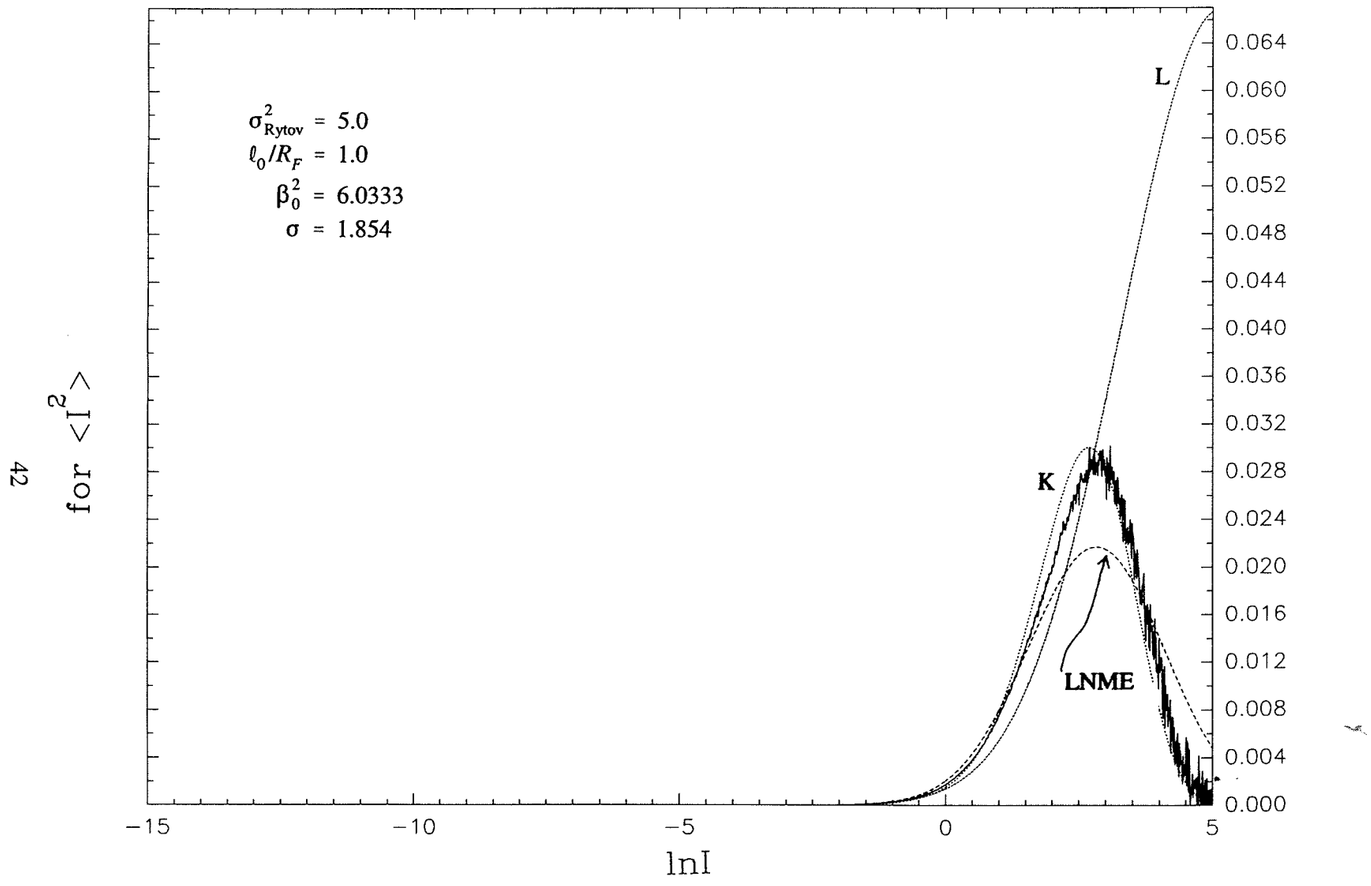

FIGURE 9c. Integrands for $f = I^2$.

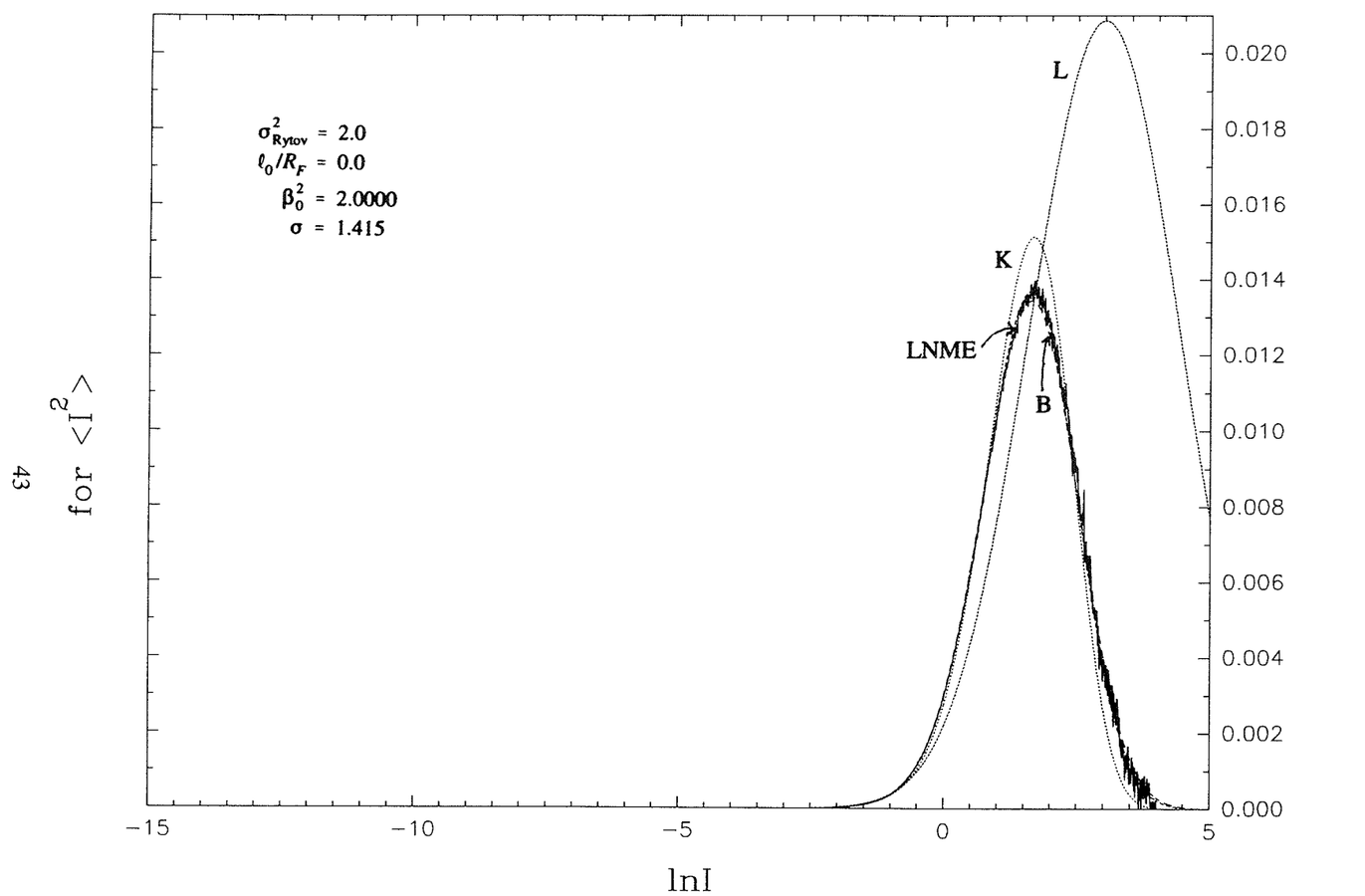

FIGURE 9d. Integrands for $f = I^2$.

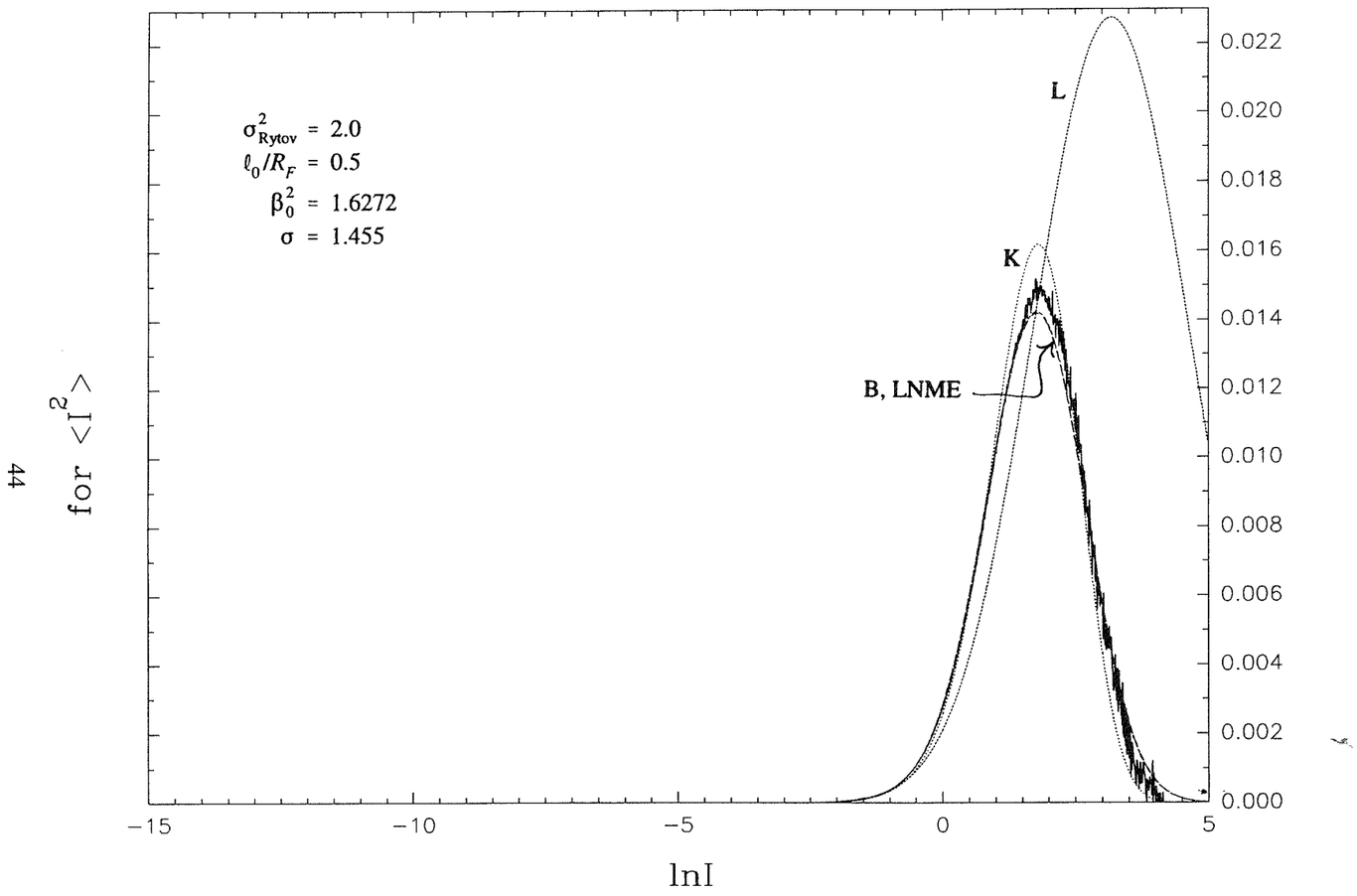

FIGURE 9e. Integrands for $f = I^2$.

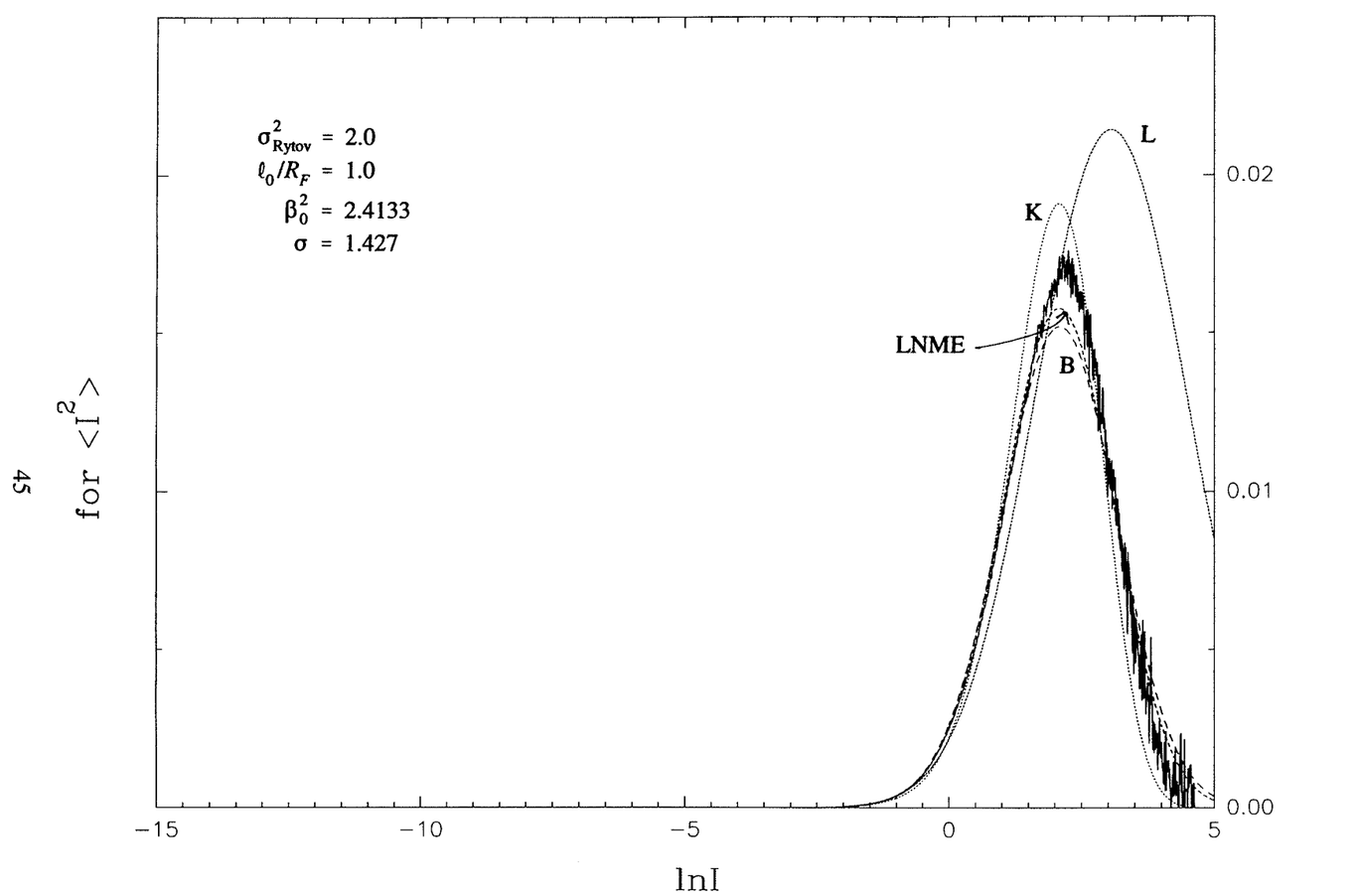

FIGURE 9f. Integrands for $f = I^2$.

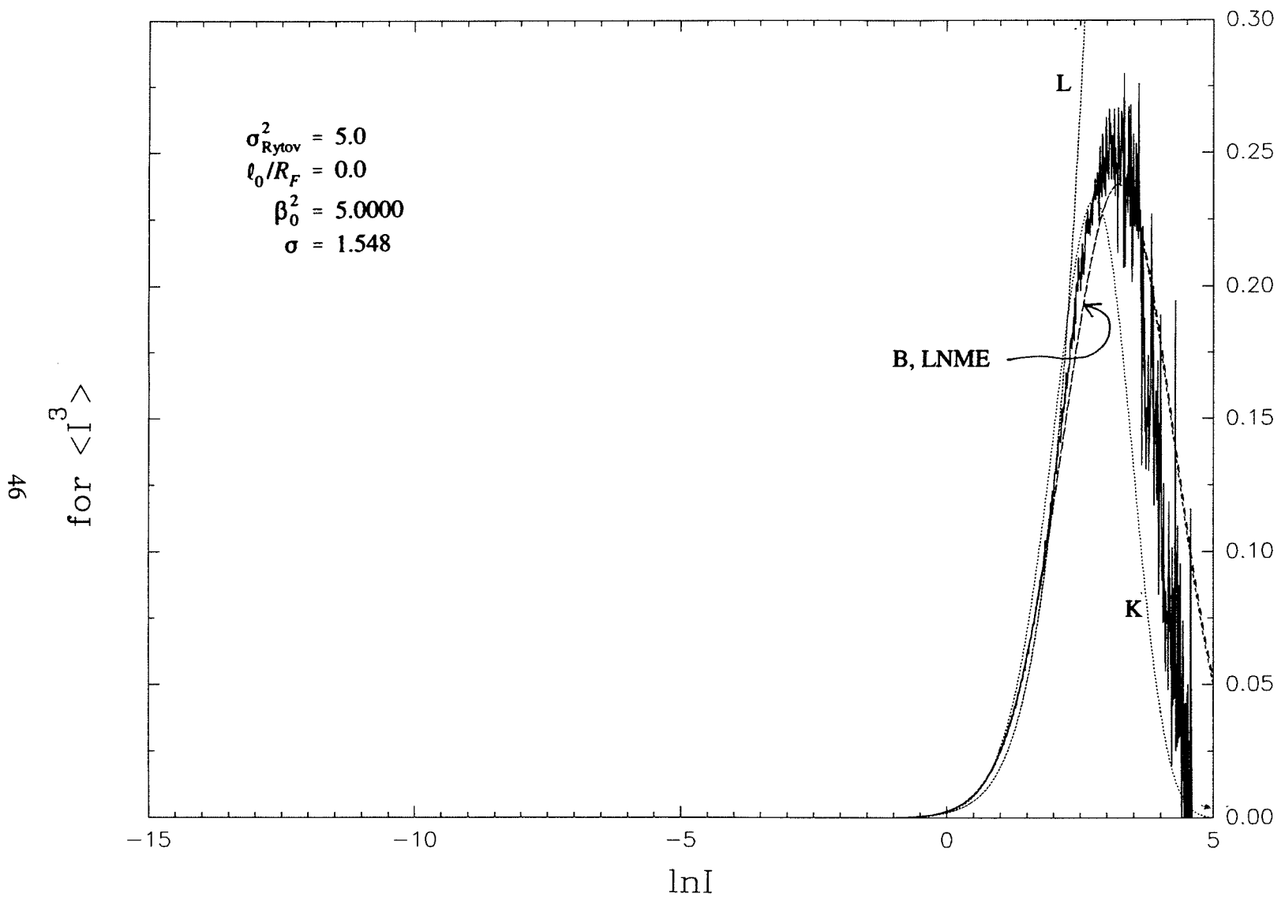

FIGURE 10a. Integrands for $f = I^3$.

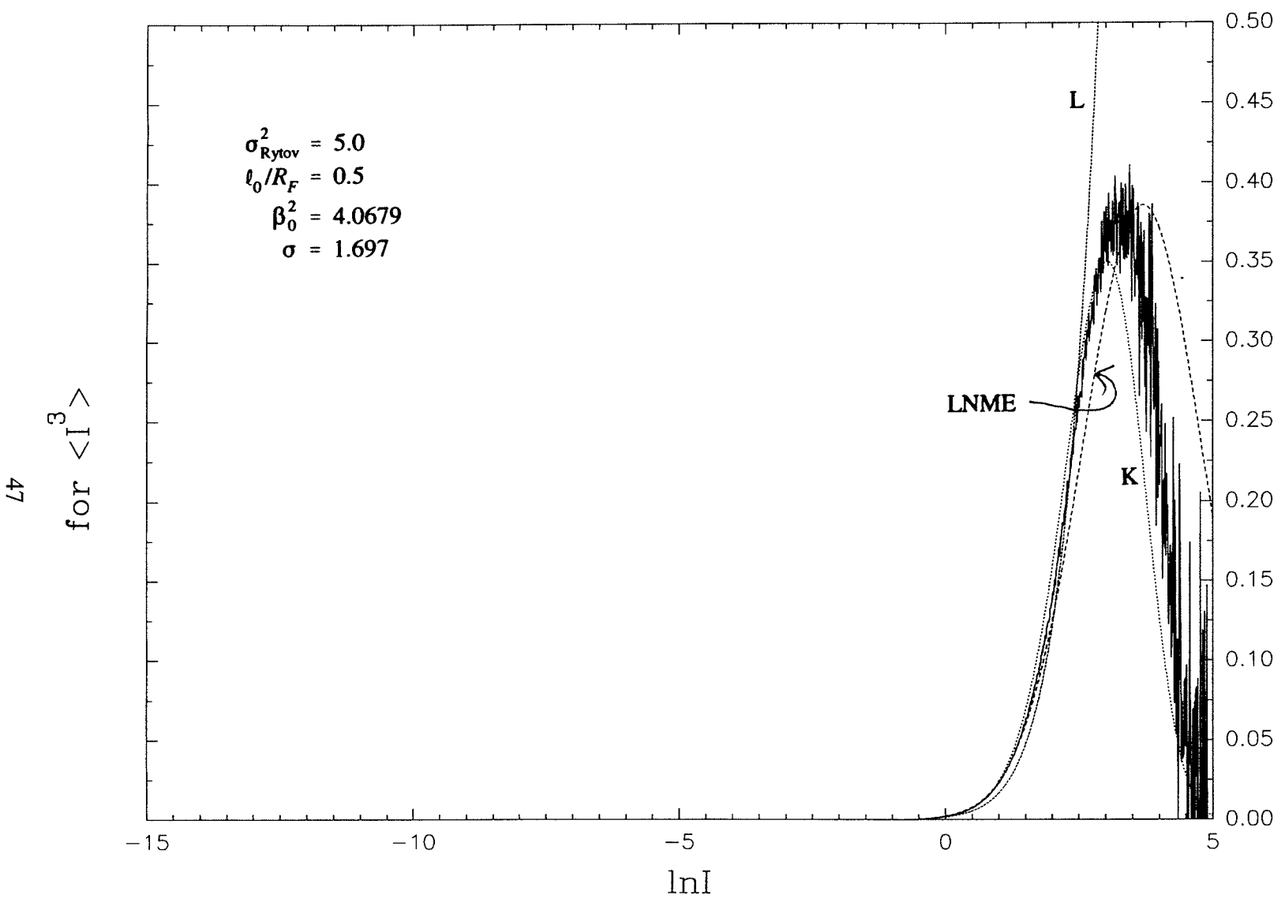

FIGURE 10b. Integrands for $f = I^3$.

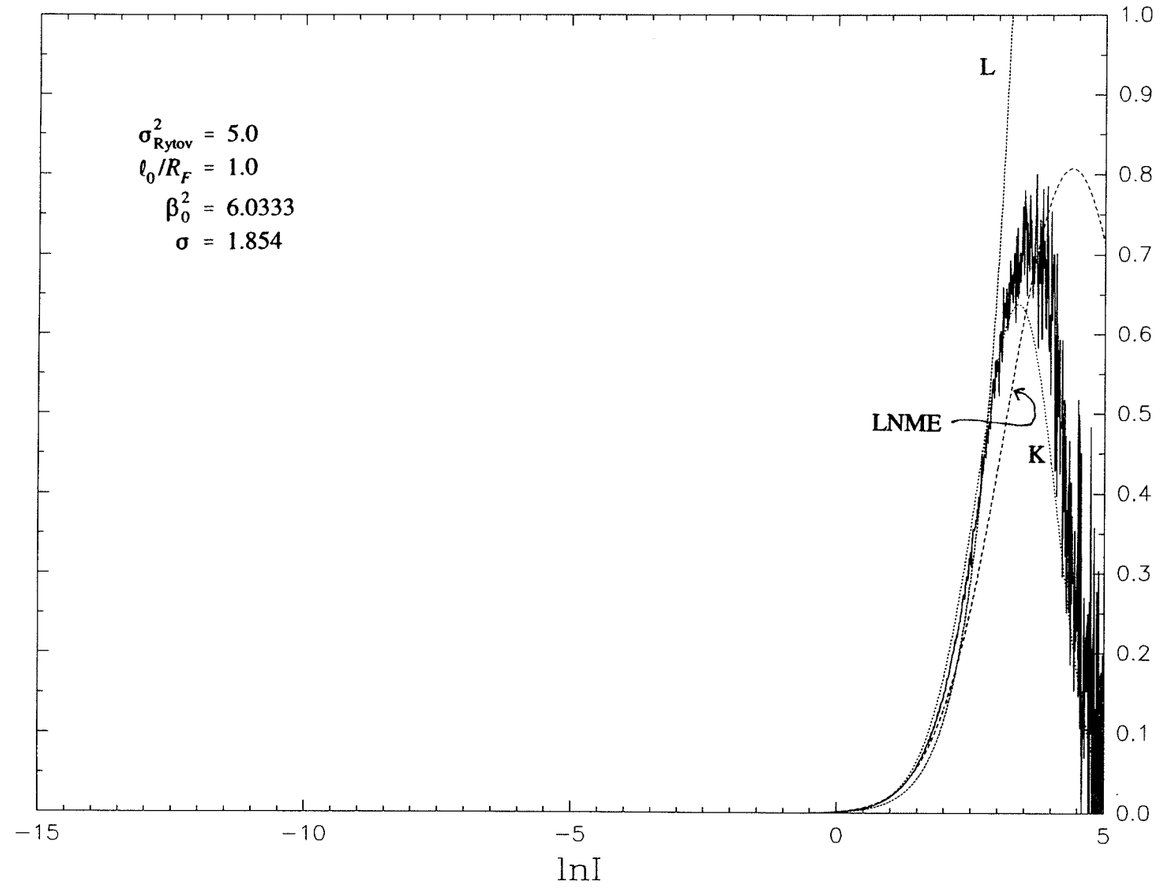

FIGURE 10c. Integrands for $f = I^3$.

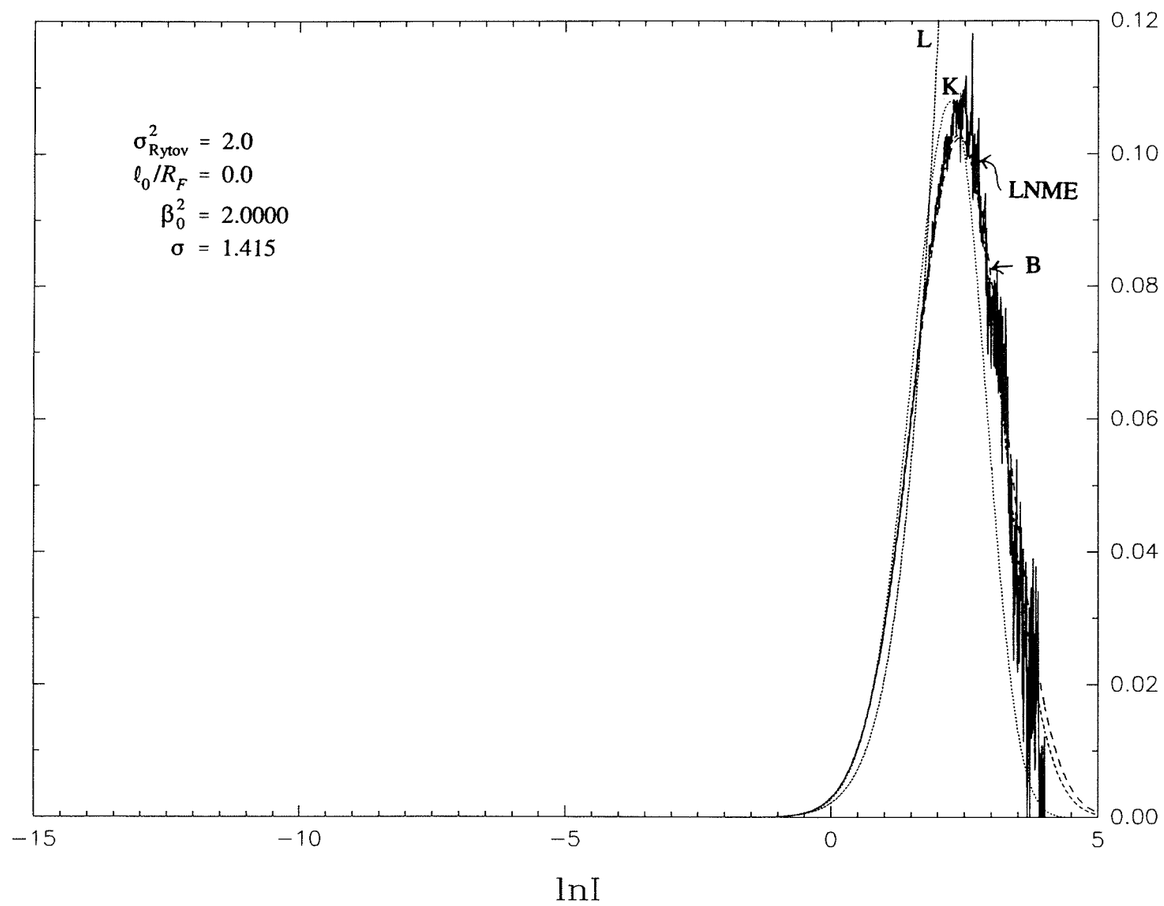

FIGURE 10d. Integrands for $f = I^3$.

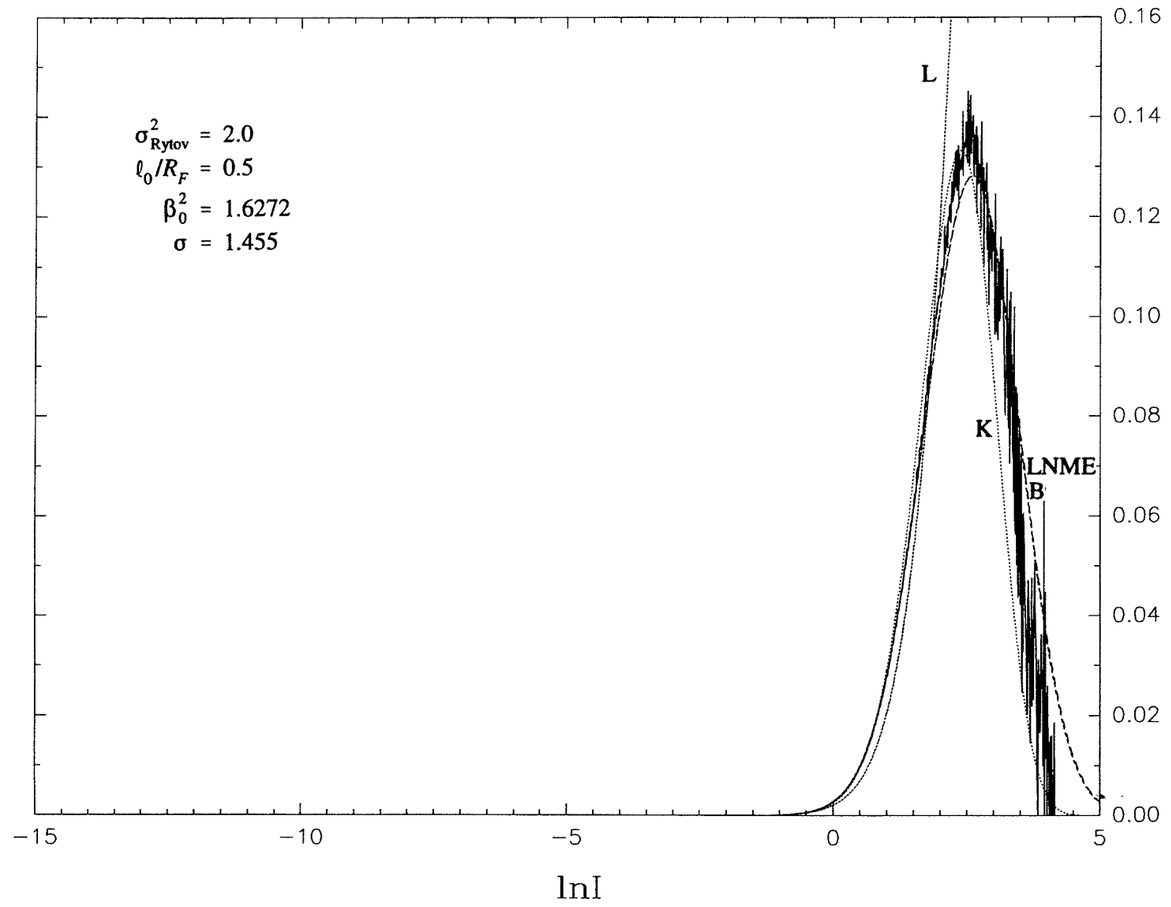

FIGURE 10e. Integrands for $f = I^3$.

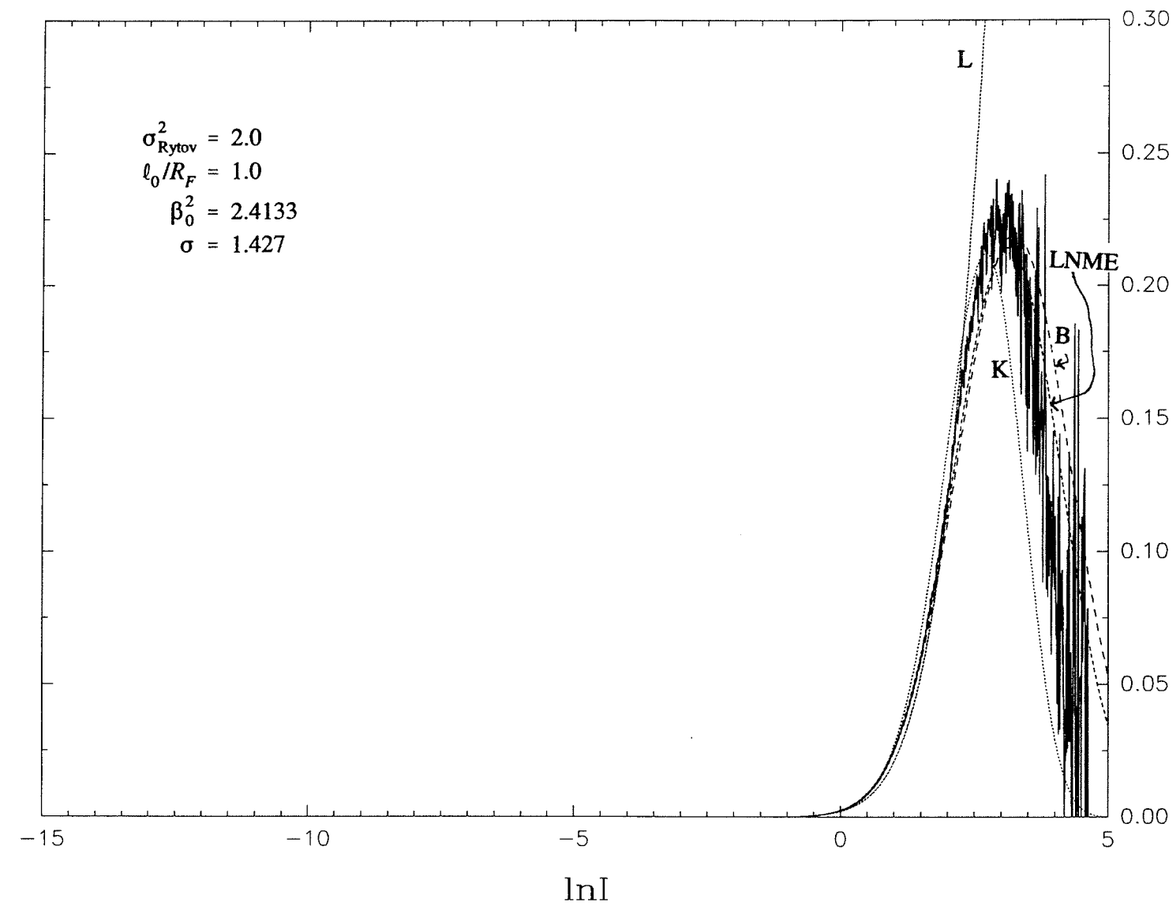

FIGURE 10f. Integrands for $f = I^3$.

TABLE 4. Statistics obtained by numerical integration of the various PDFs. Column labels corresponding to different PDFs: S is simulation; B is Beckmann's PDF; LNME is lognormally modulated exponential; L is lognormal; and K is K PDF. The ordered triples above these column labels are the values of $(\sigma^2_{\text{Rytov}}, \ell_0/R_F, \beta_0^2)$.

	(0.06, 0.0, 0.0600)						(0.06, 0.5, 0.0488)						(0.06, 1.0, 0.0724)					
	S	S	B	LNME	L	K	S	S	B	LNME	L	K	S	S	B	LNME	L	K
$\langle \ln I \rangle$	-0.030	±0.0002	**	§	-0.030	§	-0.030	±0.0002	-0.030	§	-0.030	§	-0.030	±0.0002	**	§	-0.030	§
σ^2	0.060*	±0.0003	0.061	§	**	§	0.061*	±0.0004	0.061	§	**	§	0.060*	±0.0004	0.060	§	**	§
$\langle I^{-1/2} \rangle$	1.023	##	1.023	§	1.023	§	1.023	##	1.023	§	1.023	§	1.023	##	1.023	§	1.023	§
$\langle I^2 \rangle$	1.060	±0.0003	**	§	1.062	§	1.061	±0.0004	1.061	§	1.063	§	1.062	±0.0005	**	§	1.062	§
$\langle I^3 \rangle$	1.190	##	1.190	§	1.199	§	1.193	##	1.193	§	1.200	§	1.197	##	1.197	§	1.198	§
	(1.00, 0.0, 1.0000)						(1.00, 0.5, 0.8136)						(1.00, 1.0, 1.2067)					
	S	S	B	LNME	L	K	S	S	B	LNME	L	K	S	S	B	LNME	L	K
$\langle \ln I \rangle$	-0.480	±0.002	**	-0.595	-0.602	†	-0.491	±0.003	**	-0.618	-0.588	-0.621	-0.493	±0.002	**	-0.672	-0.530	-0.685
σ^2	1.204*	±0.007	1.214	1.680	**	†	1.177*	±0.009	1.204	1.727	**	1.734	1.060*	±0.005	1.081	1.834	**	1.876
$\langle I^{-1/2} \rangle$	1.540	##	1.546	1.795	1.571	†	1.527	##	1.544	1.827	1.555	1.831	1.476	##	1.485	1.901	1.488	1.926
$\langle I^2 \rangle$	2.071	±0.011	**	**	3.328	†	2.171	±0.017	**	**	3.239	**	2.417	±0.012	**	**	2.883	**
$\langle I^3 \rangle$	7.598	##	7.663	6.658	#	†	8.684	##	8.946	7.672	33.131	7.625	12.315	##	13.031	10.583	23.722	10.269
	(2.00, 0.0, 2.0000)						(2.00, 0.5, 1.6272)						(2.00, 1.0, 2.4133)					
	S	S	B	LNME	L	K	S	S	B	LNME	L	K	S	S	B	LNME	L	K
$\langle \ln I \rangle$	-0.774	±0.003	**	-0.790	-1.001	-0.866	-0.836	±0.004	**	-0.838	-1.058	-0.956	-0.888	±0.006	**	-0.943	-1.019	-1.206
σ^2	2.003*	±0.008	2.016	2.071	**	2.341	2.117*	±0.011	2.160	2.166	**	2.611	2.039*	±0.014	2.168	2.377	**	3.483
$\langle I^{-1/2} \rangle$	2.037	##	2.043	2.078	2.118	2.258	2.125	##	2.149	2.153	2.211	2.472	2.096	##	2.184*	2.330	2.147	#
$\langle I^2 \rangle$	3.062	±0.028	**	**	#	**	3.367	±0.033	**	**	#	**	4.158	±0.059	**	**	#	**
$\langle I^3 \rangle$	21.164§§	##	22.121	21.528	#	18.945	26.427§§	##	28.673	28.563	#	23.911	47.886§§	##	#	#	#	39.383

TABLE 4. continued.

	(5.00, 0.0, 5.0000)						(5.00, 0.5, 4.0679)						(5.00, 1.0, 6.0333)					
	S	S	B	LNME	L	K	S	S	B	LNME	L	K	S	S	B	LNME	L	K
$\langle \ln I \rangle$	-0.970	±0.004	-0.960	-0.964	-1.198	-1.264	-1.162	±0.005	††	-1.058	-1.441	-1.569	-1.415	±0.008	††	-1.197	-1.719	#
σ^2	2.398*	±0.007	2.406	2.418	**	3.714	2.883*	±0.01	††	2.607	**	#	3.441*	±0.02	††	2.884	**	#
$\langle I^{-1/2} \rangle$	2.360	##	**	2.367	2.456	#	2.774	##	††	2.540	2.946	#	3.350	##	††	2.817	3.629	#
$\langle I^2 \rangle$	4.336	±0.06	**	**	#	**	5.235	±0.08	††	**	#	**	6.914	±0.11	††	**	#	**
$\langle I^3 \rangle$	52.098§§	##	#	#	#	43.381	76.972§§	##	††	#	#	66.491	138.085§§	##	††	#	#	#

§Not calculated because these PDFs are undefined for $\langle I^2 \rangle < 2.0$.

§§The moment integrands indicate that the simulation's value of $\langle I^3 \rangle$ is an underestimate.

*This value is used to scale the ordinates and abscissas of the figures.

**The simulation's value of this statistic was used to determine the parameter(s) of the PDF.

#The moment integrands show that the value of this statistic is affected by the limited range of the numerical integration. Analytic formulas could be used to obtain the statistic.

##Not calculated.

†Not computed because of problems with the computer routine for modified Bessel functions of very large order. Since $\langle I^2 \rangle$ is very close to 2.0, the K PDF is very nearly the same as the LNME and exponential PDFs.

††The parameters of Beckmann's PDF could not be determined for this case. Beckmann's PDF can be taken to be the LNME PDF.

statistic over all the realizations. These errors are indicative of the variability between realizations, but they are not confidence limits. Confidence limits require knowledge of the sample distribution of the statistic.

8. SUMMARY

We have calculated the PDFs of initially spherical waves propagating through homogeneous, nonintermittent atmospheric turbulence using numerical simulations. We compare these PDFs from simulations with several heuristic PDF models, namely, the LNME, K, lognormal, and Beckmann's PDFs. Since Beckmann's PDF is relatively unknown, we investigate it in detail. In particular, we investigate its asymptotic formulas for weak and strong scintillation, derive formulas for several of its statistics, and determine its parameters from statistics calculated from simulations. In particular, we obtain analytic formulas for $\langle \ln I \rangle_B$ and $\langle I^n \rangle_B$, where n is an integer, and $\langle I^{\mu - 1/2} \rangle_B$, where μ is a real number such that $\mu - 1/2 > -1$. Beckmann's PDF is superior to the lognormal and K PDFs when compared to the simulations' PDFs. Beckmann's PDF evolves into the LNME PDF for cases of strong scintillation; in fact, we show that Beckmann's PDF has become nearly indistinguishable from the LNME PDF for $\sigma^2_{Rytov} \geq 2.0$. Deriving the parameters of Beckmann's PDF from two statistics is found to fail for strong scintillation, but Beckmann's PDF has already closely approached the LNME PDF for these cases. For such cases, one should take the LNME PDF as the replacement of Beckmann's PDF.

9. ACKNOWLEDGMENTS

This work was partially supported by the National Science Foundation, the Army Research Office, and the National Aeronautics and Space Administration, Marshall Space Flight Center, under Research Grant NAG8-253 (Michael Kavaya, Technical Officer).

10. REFERENCES

Abramowitz, M., and I. A. Stegun, 1964. *Handbook of Mathematical Functions with Formulas, Graphs, and Mathematical Tables*. National Bureau of Standards, Applied Mathematics Series 55. U.S. Gov't. Printing Office, Washington, DC, 1046 pp.

Andrews, L., and R. Phillips, 1985. *I–K* distribution as a universal propagation model of laser beams in atmospheric turbulence. *J. Opt. Soc. Am. A* 2:160–163.

Azoulay, E., V. Thiermann, A. Jetter, A. Kohnle, and Z. Azar, 1988. Optical measurements of the inner scale of turbulence. *J. Phys. D: Appl. Phys.* 21:541–544.

Beckmann, P., 1967. *Probability in Communication Engineering*. Harcourt, Brace, and World, New York, 511 pp.

Churnside, J. H., and S. F. Clifford, 1987. Lognormal Rician probability-density function of optical scintillations in the turbulent atmosphere. *J. Opt. Soc. Am. A* 4:1923–1930.

Churnside, J. H., and R. G. Frehlich, 1989. Experimental evaluation of lognormally modulated Rician and IK models of optical scintillation in the atmosphere. *J. Opt. Soc. Am. A* 6:1760–1766.

Churnside, J. H., and R. J. Hill, 1987. Probability density of irradiance scintillations for strong path-integrated refractive turbulence. *J. Opt. Soc. Am. A* 4:727–733.

Clifford, S. F., G. R. Ochs, and R. S. Lawrence, 1974. Saturation of optical scintillation by strong turbulence. *J. Opt. Soc. Am.* 64:148–154.

Coles, W. A., J. P. Filice, R. G. Frehlich, and M. Yadlowsky, 1995. Simulation of wave propagation in three-dimensional random media. *Appl. Opt.* 34:2089–2101.

Consortini, A., F. Cochetti, J. H. Churnside, and R. J. Hill, 1993. Inner-scale effect on irradiance variance measured for weak-to-strong atmospheric scintillation. *J. Opt. Soc. Am. A* 10:2354–2362.

Fante, R. L. 1975. Electromagnetic beam propagation in turbulent media. *Proc. IEEE* 63:1669–1692.

Flatté, S. M., G.-Y. Wang, and J. Martin, 1993. Irradiance variance of optical waves through atmospheric turbulence by numerical simulation and comparison with experiment. *J. Opt. Soc. Am. A* 10:2363–2370.

Flatté, S. M., C. Bracher, and G.-Y. Wang, 1994. Probability-density functions of irradiance for waves in atmospheric turbulence calculated by numerical simulation. *J. Opt. Soc. Am. A* 11:2080–2092.

Frehlich, R. G., 1992. Laser scintillation measurements of the temperature spectrum in the atmospheric surface layer. *J. Atmos. Sci.* 49:1494–1509.

Gracheva, M. E., A. S. Gurvich, S. S. Kashkarov, and V. V. Pokasov, 1974. Similarity relations for strong fluctuations of light in a turbulent medium. *Zh. Eksp. Teor. Fiz.* 67:2035–2046. [English translation: *Sov. Phys. JETP* 40:1011–1016, 1974.]

Gradshteyn, I. S., and I. M. Ryzhik, 1965. *Table of Integrals, Series, and Products*. Academic Press, New York, 1086 pp.

Hill, R. J., 1982. Theory of saturation of optical scintillation by strong turbulence: plane-wave variance and covariance and spherical-wave covariance. *J. Opt. Soc. Am.* 72:212–221.

Hill, R. J., 1992. Review of optical scintillation methods of measuring the refractive-index spectrum, inner scale, and surface fluxes. *Waves in Random Media* 2:179–201.

Hill, R. J., and S. F. Clifford, 1978. Modified spectrum of atmospheric temperature fluctuations and its application to optical propagation. *J. Opt. Soc. Am.* 68:892–899.

Hill, R. J., and S. F. Clifford, 1981. Theory of saturation of optical scintillation by strong turbulence for arbitrary refractive-index spectra. *J. Opt. Soc. Am.* 71:675–685.

Hill, R. J., and R. G. Frehlich, 1996. Onset of strong scintillation with application to remote sensing of turbulence inner scale. *Appl. Opt.* 35:986–997.

Hill, R. J., and G. R. Ochs, 1978. Fine calibration of large-aperture optical scintillometers and an optical estimate of the inner scale of turbulence. *Appl. Opt.* 17:3608–3612.

Hill, R. J., R. A. Bohlander, S. F. Clifford, R. W. McMillan, J. T. Priestley, and W. P. Schoenfeld, 1988. Turbulence-induced millimeter-wave scintillation compared with micrometeorological measurements. *IEEE Trans. Geosci. Remote Sens.* 26:330–342.

Hill, R. J., W. D. Otto, and J. R. Jordan, 1994. Operation of the fluxes scintillometer. NOAA Tech. Memo. ERL ETL-241, NOAA Environmental Research Laboratories, Boulder, CO. [Available from the National Technical Information Service, 5285 Port Royal Rd., Springfield, VA 22161.]

Jakeman, E., and P. Pusey, 1978. Significance of *K* distributions in scattering experiments. *Phys. Rev. Lett.* 40:546–550.

Lawrence, R. S., and J. W. Strohbehn, 1970. A survey of clear air propagation effects relevant to optical communication. *Proc. IEEE* 58:1523–1545.

Little, C. G., 1951. A diffraction theory of the scintillation of stars on optical and radio wavelengths. *Mon. Not. R. Astron. Soc.* 111:289–302.

Milyutin, E. R., and Yu. I. Yaremenko, 1980. Distribution of intensity fluctuation in optical radiation propagating in a turbulent atmosphere. *Radiotekhnika i Elektronika* 25:2272–2278. [English translation: *Radio Eng. Electron. Phys.* 25:1–5, 1980.]

Nakagami, M., 1960. The *m*-distribution—A general formula of intensity distribution of rapid fading. In *Statistical Methods in Radio Wave Propagation*. W. C. Hoffman (Ed.), Pergamon, New York, 3–36.

Ochs, G. R., and Hill, R. J., 1985. Optical-scintillation method of measuring turbulence inner scale. *Appl. Opt.* 24:2430–2432.

Prudnikov, A. P., Yu. A. Brychkov, and O. I. Marichev, 1986. *Integrals and Series. Volume 2. Special Functions.* Gordon and Breach Science Publishers, New York, 750 pp.

Strobehn, J. W., T. Wang, and J. P. Speck, 1975. On the probability distribution of line-of-sight fluctuations of optical signals. *Radio Sci.* 10:59–70.

Thiermann, V., and H. Grassl, 1992. The measurement of turbulent surface-layer fluxes by use of bichromatic scintillation. *Boundary-Layer Meteorol.* 58:367–389.

APPENDIX

Churnside and Clifford (1987) independently derived Beckmann's PDF. They obtained the parameters r and σ_z^2 from the heuristic theory of Hill and Clifford (1981). That heuristic theory is, in turn, a generalization of the heuristic theory of Clifford et al. (1974). Hill and Frehlich (1996) showed that the heuristic theory gives values of log-irradiance variance that are in error by as much as 33%. However, Churnside and Clifford (1987) used the heuristic theory in a novel way to determine r and σ_z^2, so we must examine errors caused by use of the heuristic theory. For several selected values of σ_{Rytov}^2, we read Fig. 2 in Churnside and Clifford (1987) to obtain their values of σ_z^2 for the case $\ell_0 = 0$. This is the only case for which they graph σ_z^2; it is also the only case that coincides with our simulations because they used an *ad hoc* model for $H(\kappa \ell_0)$, which is the dimensionless function that describes the bump and dissipation range of the refractive-index spectrum. We obtain their value of r from Eq. (26) in Churnside and Clifford (1987). These values are presented in Table A1. Table A1 also gives the corresponding values of r and σ_z^2 as determined from the simulation; these values are rounded values from Table 1. Also given in Table A1 are the values of irradiance variance $\sigma_I^2 = \langle I^2 \rangle - 1$, as obtained using (14). Table A1 shows the errors in r and σ_z^2 caused by use of the heuristic theory. Table A1 also shows that the resulting error in irradiance variance increases as the condition of strong focusing is approached.

TABLE A1. Comparison of r and σ_z^2 determined from the heuristic theory with r and σ_z^2 from the simulation. Values of σ_I^2 from (14) are given.

	Heuristic theory			Simulation		
σ_{Rytov}^2	r	σ_z^2	σ_I^2	r	σ_z^2	σ_I^2
0.4	5.79	0.12	0.44	7.46	0.15	0.42
1.00	2.05	0.20	0.89	2.41	0.32	1.1
2.00	0.822	0.34	1.5	0.629	0.50	2.1
5.00	0.158	0.57	2.5	0.329	0.81	3.3

*U.S. GOVERNMENT PRINTING OFFICE 1997-0-573-018/40035